The Functional Role of the Mammalian Tectorial Membrane in Cochlear Mechanics

by

Roozbeh Ghaffari

Submitted to the Harvard–Massachusetts Institute of Technology
Division of Health Sciences and Technology
in partial fulfillment of the requirements for the degree of

Doctor of Philosophy

at the

MASSACHUSETTS INSTITUTE OF TECHNOLOGY

February 2008
January 2008

Author .....
Harvard–Massachusetts Institute of Technology Division of Health Sciences and Technology
January, 2008

Certified by .....
Dennis M. Freeman
Professor of Electrical Engineering
Thesis Supervisor

Accepted by .....
Martha L. Gray
Edward Hood Taplin Professor of Medical and Electrical Engineering
Director, Harvard-MIT Division of Health Sciences and Technology

The Functional Role of the Mammalian Tectorial Membrane in Cochlear Mechanics

by

Roozbeh Ghaffari

Submitted to the Harvard–Massachusetts Institute of Technology Division of Health Sciences and Technology
on January, 2008, in partial fulfillment of the requirements for the degree of Doctor of Philosophy

Abstract

Sound-evoked vibrations transmitted into the mammalian cochlea produce traveling waves that provide the mechanical tuning necessary for spectral decomposition of sound. These traveling waves of motion propagate along the basilar membrane (BM) and ultimately stimulate the mechano-sensory receptors. The tectorial membrane (TM) plays a key role in this stimulation process, but its mechanical function remains unclear. Here we show that the TM supports traveling waves that are an intrinsic feature of its visco-elastic structure. Radial forces applied at audio frequencies (1-20 kHz) to isolated TM segments generate longitudinally propagating waves on the TM with velocities similar to those of the BM traveling wave near its best frequency (BF) place. We compute the dynamic shear storage modulus and shear viscosity of the TM from the propagation velocity of the waves and show that segments of the TM from the basal turn are stiffer than apical segments are. Analysis of loading effects of hair bundle stiffness, the limbal attachment of the TM, and viscous damping in the subtectorial space suggests that TM traveling waves can occur *in vivo*.

To test how TM waves may participate in cochlear function, we investigated waves in genetically modified mice lacking beta-tectorin, a glycoprotein found exclusively in the TM. $Tectb^{-/-}$ mutant mice were previously shown to exhibit significant loss of cochlear sensitivity at low frequencies and sharpened frequency tuning compared to wild types. We show that the spatial extent and propagation velocity of TM traveling waves are significantly reduced in $Tectb^{-/-}$ mice compared to wild types, consistent with the concept that there is a reduction in the spread of excitation via TM waves and less TM wave interaction with the BM traveling wave in $Tectb^{-/-}$ mice. The differences in TM wave properties between mutants and wild types arise from changes to the mechanical properties of the TM; mutant TMs are significantly less stiff than wild type TMs are. Our results show the presence of a traveling wave mechanism through the TM that can functionally couple a significant longitudinal extent of the cochlea and may interact with the BM wave, suggesting that TM waves are crucial for cochlear sensitivity and tuning.

Thesis Supervisor: Dennis M. Freeman
Title: Professor of Electrical Engineering

Acknowledgments

There are several individuals who have devouted countless hours to helping me over the past six years. Without their help, guidance, and wisdom, this document would not have come to fruition. First and foremost, I want to thank my advisor and friend, Denny Freeman, for playing a very active role in my research and for helping me mature as an experimental researcher. Denny has taught me everything I know about tackling scientific questions and about conducting scientific research. I am looking forward to continuing our personal and professional relationship in the years to come. I'd also like to recognize my committee members, John Guinan and Alan Grodzinsky. About three years ago, I presented some rough wave measurement data as an afterthought during a committee meeting and it was at this meeting that Alan Grodzinsky recognized that tectorial membrane material properties could be characterized from these waves. John Guinan has been absolutely incredible as chair of my committee. He has met with me on several occasions ($n > 30$), usually for two to three hours to discuss my research. He has been a great friend and mentor throughout this entire process. Christopher Shera also has advised me on several occasions and has read and critiqued several drafts of my thesis work. His points and comments have been invaluable in helping get my research published. Finally, AJ Aranyosi has been a great friend and mentor. This thesis was completed because of the countless hours AJ devouted to the projects covered in this document. I will never forget the years that we have spent working together as a team.

I've worked with several inspiring and brilliant graduate students and staff members during my years in graduate school. Kinu Masaki was the best office mate I could have asked for. She introduced me to the Speech and Hearing Bioscience and Technology Program and told me countless times to apply. I am now graduating from this same program 5 years later. Wendy Gu, Scott Page, Chris Bergevin, Stan Hong, Salil Desai, Micheal Vahey, Luke Theogarajan, Ying-Chi Wang, and J. Ryu have provided much-needed research support and feedback on posters, talks, and papers over the years. Janice Balzer has been very helpful behind the scenes, keeping our my lab

functioning day to day.

I'd also like to acknowledge the individuals who have been my closest friends and supporters throughout this entire process: Patsy Wilson, Emelio Williams, Ayanna Samuels, Amanda Graves, Jamy Drouillard, Nikhil Sadarangani, Jimmy Lin, Abishek Singh, Donna Destouche, Ashok Sivakumar, Reuben Cummings, Adrienne Manns, Matthew Malcolm, Deverraux Jones, Junior Desrosier, and Shounak Lahiri.

Finally, I'd like to thank the individuals in my life who have been around from the very beginning, before I even set foot in Cambridge. My parents, Pari and Daryoush Ghaffari have dedicated their lives to helping me succeed in mine. And my younger brother, Soran Ghaffari, whose life has been an inspiration for me ever since his birth. Without you, I would not have made it this far.

Contents

List of Figures

Chapter 1

Introduction

"The theories in which the basilar membrane is considered the vibrating mechanism in the cochlea are considered untenable, and an application of the telephone theory to the tectorial membrane as the vibrating mechanism is suggested on the basis of its logical position, its extent, shape, proportions, consistency and structure, and the probable character of the transformed and transferred sound waves in the endolymph of the cochlea." Irving Hardesty, 1908

The mammalian cochlea is a remarkable sensor that can detect motions significantly smaller than the diameter of a hydrogen atom and can perform high quality spectral analysis to discriminate as many as 30 frequencies in the interval of a single semi-tone (Kössl and Russell, 1995; Dallos, 1996). These extraordinary properties of the hearing organ (Figure 1-1) underpin our ability to hear a variety of sounds ranging from a pin drop to a jet engine, from a quiet whisper to music at a rock concert. Our ability to sense and distinguish between these different sounds depends on the mechanical properties and function of the cochlea.

The cochlea contains mechano-sensory receptors called hair cells (Hudspeth, 1985), which transduce sound-evoked vibrations into electrical signals that are then transmitted to the brain. While there has been extensive progress in our understanding of hair cell physiology and anatomy over the past 30 years, very little is known about a gelatinous matrix called the tectorial membrane (TM), which overlies the sensory

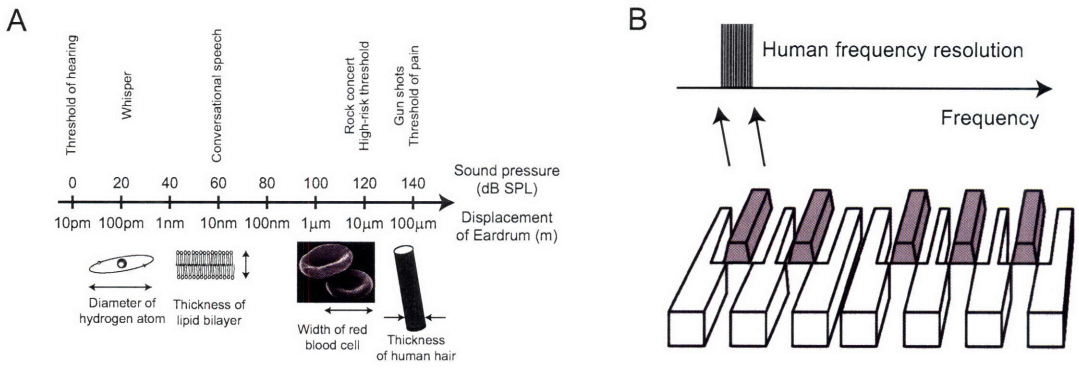

Figure 1-1: (A) The cochlea has remarkable sensitivity. It can sense sound vibrations that displace the ear drum less than the diameter of a hydrogen atom at the threshold of hearing. (B) The cochlea has exquisite frequency selectivity. It can discriminate up to 30 frequencies in the interval of a single semi-tone (two adjacent keys on the piano). Images adapted from Freeman.

hair cells. The work presented in this thesis aims to characterize the function of the mammalian TM in the cochlea to further our knowledge of cochlear mechanisms.

1.1 Cochlear Anatomy

The mammalian cochlea is a snail-shaped organ that is encased in the temporal bone, the hardest bone in the body. It consists of three fluid-filled ducts: scala vestibuli, scala media, and scala tympani, which span the entire length of the cochlea. A thin membrane called Reissner's membrane acts as a partition between scala vestibuli and scala media. Similarly, the organ of Corti separates the fluid in scala media from scala tympani (Figure 1-2). Scala media contains endolymph, a fluid high in potassium and very low in calcium ions. Scala vestibuli and tympani contain perilymph, a fluid that

is high in sodium, typical of extracellular fluids. The TM resides in scala media, directly above the organ of Corti. The basilar membrane (BM) is situated on the side opposite to the TM, directly underneath the organ of Corti.

The organ of Corti houses the sensory hair cells of the cochlea. There are two types of cochlear hair cells: the inner hair cells (IHCs) and the outer hair cells (OHCs). The IHCs act as sensory receptors that detect and transmit sound stimuli to the brain via afferent nerve fibers. In contrast, the OHCs are predominantly innervated by efferent nerve fibers and are electromotile (Brownell et al., 1985; Kennedy et al., 2005). It is widely believed that OHC electromotility plays a key role in boosting cochlear sensitivity and frequency selectivity. Both types of hair cells project densely–packed arrays of stereocilia from their apical surface forming a hair bundle, the receptor site of the hair cell. Hair bundles contain approximately 20–300 stereocilia, each housing mechanically sensitive transduction channels that open and close in response to mechanical stimuli in the radial direction (Hudspeth, 1985). The TM contacts the OHCs at the tips of their stereociliary hair bundles (Lim, 1972) and hovers directly above the IHC bundles (Figure 1-2).

1.2 Cochlear Function

Sound-evoked vibrations are transmitted through the external and middle ears before they enter the cochlea. The middle ear contains three bones that are coupled to a thin membrane called the oval window, which is located at the entrance (base) of the cochlea. Acoustic energy causes the middle ear bones to move like pistons, which in turn vibrates the oval window. These vibrations launch a traveling wave that propagates from the base to the apex of the cochlea (Figure 1-3). von Békésy demonstrated that these waves propagate along the basilar membrane (BM) in his seminal research on the ears of human cadavers (von Békésy, 1960). He showed that the cochlea maps frequency to position along its length (Robles and Ruggero, 2001) such that each traveling wave propagates to a characteristic place, where it peaks in amplitude and rapidly decays at locations immediately apical to the characteristic

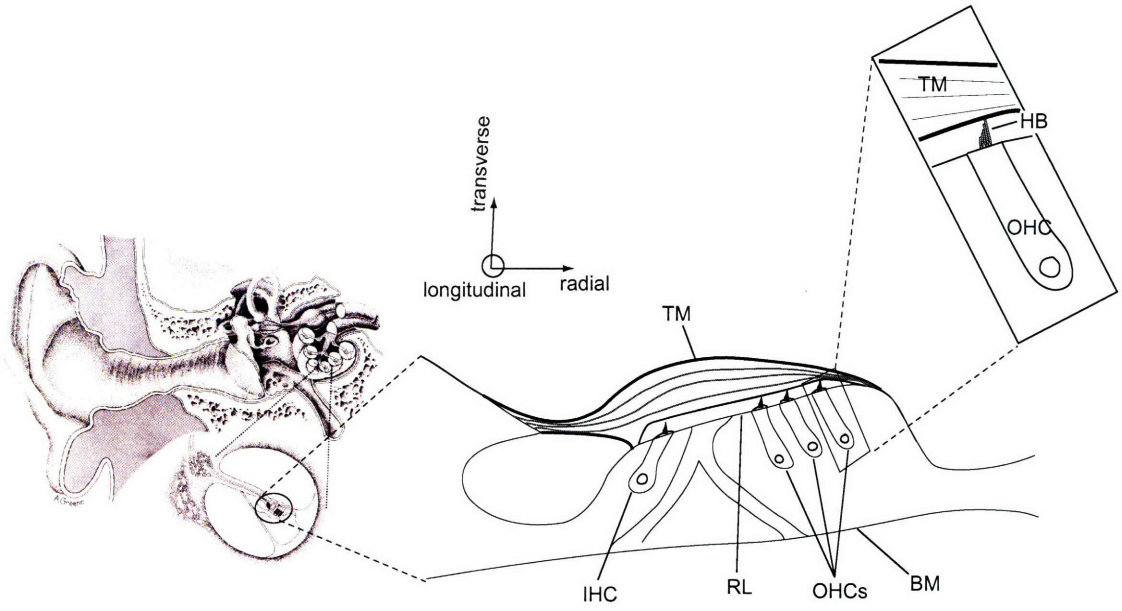

Figure 1-2: Left: Schematic drawing of the cochlea in the inner ear (drawing by Anne Greene). Middle: Schematic drawing of the cochlear partition (adapted from (Abnet, 1998)). The TM overlies the stereociliary bundles of the sensory hair cells. The sensory hair cells and supporting cells (not shown) are situated on the basilar membrane (BM). The narrow space between the undersurface of the TM and the reticular lamina (RL) is known as the subtectorial space. Right: The tips of the OHC hair bundles (HB) contact the bottom surface of the TM.

place. All frequencies in the audible range have a characteristic place along the cochlea. High frequency sounds peak near the base of the cochlea and low frequency sounds travel further along the cochlear spiral towards the apex (Figure 1-3).

As acoustic energy propagates along the length of the cochlea, it creates a pressure difference across the BM. This pressure difference displaces the BM in the transverse direction and is believed to cause shearing between the apical surface of hair cells and the TM (Figure 1-3) that deflects the hair bundles. The TM is intimately involved in this stimulation process, but its mechanical function remains unclear.

1.3 The Mammalian Tectorial Membrane

1.3.1 The TM is a Polyelectrolyte Gel

Biochemical studies of the TM over the past 20 years have revealed that the TM is a polyelectrolyte gel (Weiss and Freeman, 1997b; Freeman, Masaki, McAllister, Wei and Weiss, 2003). It is comprised of a porous matrix of highly charged glycosaminoglycans (GAGs), glycoproteins (alpha-tectorin, beta-tectorin, and otogelin), collagen, and water (97% of total weight) (Richardson et al., 1987; Thalmann et al., 1987; Suzuki et al., 1992; Thalmann et al., 1993; Killick et al., 1995).

Collagen Matrix

Type II collagen is the most abundant type of collagen found in the TM. These collagens form fibrils that are aligned in the radial direction in the TM. In various other types of connective tissues, collagen fibrils provide tensile strength (Eyre and Wu, 1995). Other types of collagen that have been identified in the TM include types V, IX, and XI, which are minor structural constituents compared to type II collagen. Nevertheless, these other types of collagen contribute to the structural organization of the TM by mediating the inter-fibrillar spacing and the interaction of type II collagen with macromolecules (Mendler et al., 1989; Eikenberry et al., 1991; Li et al., 1995).

Glycosaminoglycans

Glycosaminoglycans (GAGs) are polysaccharide chains that are covalently bonded to a core protein. They contain sulfated and carboxylated sugars that are negatively charged. There are four types of GAGs: hyaluronan, chondroitin sulfate, heparin sulfate, and keratan sulfate (Alberts et al., 1994). The TM contains chondroitin sulfate and keratan sulfate, which comprise 9.7% and 5.7% of the TM's dry weight, respectively.

Although collagen makes up 58% of the dry weight of the TM, the contribution of GAGs to TM mechanical properties cannot be ignored (Freeman, Masaki, McAllister,

Wei and Weiss, 2003). Several previous studies have demonstrated that the mechanical, electrical, osmotic, and chemical properties of polyelectrolyte gels are interlinked and dependent on the presence of highly charged macromolecules (Frank et al., 1990; Freeman, Masaki, McAllister, Wei and Weiss, 2003). In cartilage, fixed charge has been shown to contribute to the compressive stiffness of the tissue (Buschmann and Grodzinsky, 1995), suggesting that highly charged macromolecules are poised to play an important mechanical role.

Non-Collagenous Glycoproteins: Alpha-tectorin, Beta-tectorin, Otogelin

Alpha and beta-tectorin are non-collagenous proteins found in the striated sheet matrix of the TM (Killick et al., 1995; Goodyear and Richardson, 2002). This matrix is a core structural component of the TM that has collagen fibrils embedded within it.

The genes that encode alpha-tectorin and beta-tectorin are *Tecta* and *Tectb*, respectively. Genetic mutations of the *Tecta* gene in humans and mouse models have been shown to significantly alter the structure of the TM (Legan et al., 2000; Legan et al., 2005). In homozygous mice with a mutation in *Tecta*, the TM was detached from the spiral limbus. In contrast, in heterozygous mice, the TM was still attached to the spiral limbus and to the tips of the OHC hair bundles (Legan et al., 2005). The striated sheet matrix was either missing or significantly reduced in the TMs of both homozygotes and heterozygotes. Consequently, the distribution of collagen in the TM also was disrupted.

Similar to mutations in *Tecta*, genetic mutations targeting *Tectb* have significant effects on the structure of the TM and on cochlear function. In $Tectb^{-/-}$ mutant mice, the TM remained attached to the tips of the OHC hair bundles and to the spiral limbus; however, the striated sheet matrix was missing (Russell et al., 2007). Hensen's stripe and the marginal band (in the apex) of the TM were also missing. These mutations collectively highlight the prominence of glycoproteins in the TM and demonstrate the importance of TM glycoproteins as a target of study. Chapter 3 in this thesis will explore how the *Tectb* mutation affects the mechanical properties of the TM.

Unlike alpha-tectorin and beta-tectorin, otogelin is found in other extracellular matrices in the inner ear besides the TM. The otoconial membrane and cupulae also contain otogelin. Otogelin is encoded by the *Otog* gene. A study on genetically modified $Otog^{-/-}$ mice demonstrated that otogelin is involved in organizing the fibrillar structure of the TM. These mutant mice exhibited impairments in vestibular and auditory function (Simmler et al., 2000).

1.3.2 Radial Structure of the TM

The physical structure of the TM is highly anisotropic. This anisotropy is evident in longitudinal and radial stiffness measurements of the TM (Abnet and Freeman, 2000; Gu et al., 2005). The TM is stiffer by about a factor of two in the radial direction. The radial structure of the TM is organized into three distinct zones: the limbal zone, middle zone, and the marginal zone (Lim, 1972). All three zones are visible under light microscopy as shown in Figure 1-4.

Limbal Zone

The limbal zone anchors the TM to the spiral limbus. This is the thinnest section of the TM ($\sim$10 μm). Models of this region of the TM have ranged from completely rigid to mechanically inconsequential (Abnet and Freeman, 2000).

Middle Zone

The middle zone of the TM extends over the inner and outer hair cells and is comprised of densely packed collagen fibrils oriented in the radial direction. The undersurface of the TM in the middle zone is physically attached to the tips of the OHC hair bundles (Lim, 1972) and is coupled to the IHC bundles through the fluid. The middle zone is the thickest region of the TM ($\sim$30-50 μm).

Marginal Zone

The marginal zone is the outermost region relative to the cochlear modiolus.

Why study the tectorial membrane? Based on its strategic location in the cochlea, the TM is widely believed to play a key role in stimulating hair cells. Mouse models with genetically modified structural components of the TM have been shown to exhibit severe loss of cochlear sensitivity and altered frequency tuning (McGuirt et al., 1999; Legan et al., 2000; Simmler et al., 2000; Legan et al., 2005; Russell et al., 2007), thereby providing further evidence that the TM is required for normal cochlear function. There are two glycoproteins, alpha-tectorin and beta-tectorin, which have been used to study the functional role of the TM in auditory function. In $Tecta^{Y1870C/+}$ mice, the Y1870C missense mutation of alpha-tectorin caused a significant reduction in sensitivity by 50-80 dB SPL compared to wild types while basilar membrane (BM) sensitivity decreased by ~8 dB SPL. These findings are not consistent with any previous models of the TM and suggest that the TM not only shears the OHC hair bundles but also provides the coupling that allows OHCs to enhance the stimulus to the IHCs (Legan et al., 2005).

In contrast to $Tecta^{Y1870C/+}$ mutants, mice with a targeted deletion of beta-tectorin exhibited sharpened frequency tuning and significantly lower sensitivity at low frequencies compared to normals. Although these two mutations have demonstrated that the TM is required for normal cochlear function, the mechanistic role of the TM in cochlear mechanics remains unclear, largely because the important mechanical properties of the TM have proved difficult to measure (Freeman, Masaki, McAllister, Wei and Weiss, 2003).

1.3.3 Previous Models of the TM

There are a variety of cochlear models that describe the function of the TM. Historically, the TM has been modeled as a stiff lever (with a compliant pivot at the spiral limbus) relative to the hair bundles (Davis, 1958; Johnstone and Johnstone, 1966; Billone and Raynor, 1973; Neely and Kim, 1983) as illustrated in Figure 1-5. Based on this conception, the TM is assumed to have an infinite radial and bending stiffness. In addition to the stiff lever model, the TM has been modeled as a resonant mass–spring system (Zwislocki and Kletsky, 1980; Allen, 1980; Neely and Kim, 1986) or as a mass

(Figure 1-5) (Mammano and Nobili, 1993). However, there are few mechanical measurements to support any of these models. The common underlying assumption in these 'classical' cochlear models is that the longitudinal stiffness of the TM is neglible and adjacent longitudinal sections of the cochlea are uncoupled (Figure 1-6) except for energy propagation through the fluid (de Boer, 1997).

1.3.4 Previous Measurements of TM Mechanical Properties

The earliest published mechanical measurements of the TM were conducted *in situ*. von Békésy was one of the first investigators to probe the mechanical properties of the TM by applying forces with single strands of hair. von Békésy also reported the first dynamic mechanical measurements on the TM with a vibrating needle (von Békésy, 1960). Zwislocki and Ceferrati also applied point forces to the TM by using a fine glass pipet (Zwislocki and Cefaratti, 1989). The forces exerted on the TM could be determined from the bend in the pipet. The stiffness of the TM could then be computed from the applied force and the resulting deflection of the TM. Although these measurements were the first to probe the local interaction of the TM with the hair bundles, several issues have been raised about the use of compliant probes to study the mechanical properties of the TM *in situ* (Abnet, 1998). First, the size of deformations generated by compliant probes are at least 1000× larger than the displacements that exist at the threshold of hearing. Second, poor visual access of the TM *in situ* requires the use of staining agents, which can alter the mechanical properties of the TM (Abnet and Freeman, 2000). Point forces applied to the TM *in situ* may additionally test the mechanical properties of other cochlear structures in close contact with the TM. Therefore, TM stiffness measurements are not exclusively limited to the intrinsic mechanical properties of the TM.

To address the problems of the *in situ* preparation, the most recent measurements have been conducted on isolated segments of the TM attached to a glass slide. This technique was first developed by Shah et al. (Shah et al., 1995). There are several recent studies detailing the mechanical and material properties of the TM using an isolated TM preparation. Masaki et al. (2006) applied osmotic pressure to isolated TM

segments to measure the stress-strain relation of the TM (Masaki et al., 2006). Others have extrapolated TM material properties from point indentations applied with force cantilevers to isolated TMs (Shoelson et al., 2004; Gueta et al., 2006; Richter et al., 2007). Shear forces also have been applied to isolated TM segments attached to the surface of a glass slide. Abnet and Freeman (2000) and Gu et al. (2005) applied shear forces in the radial direction with magnetic beads and custom-designed microfabricated shearing probes at audio frequencies (Gu et al., 2005; Abnet and Freeman, 2000). These dynamic measurements indicated that the TM is viscoelastic and can spatially couple motion in the radial and longitudinal directions (Gu et al., 2005; Abnet and Freeman, 2000).

1.4 Traveling Waves in Visco-elastic Structures

The fact that the TM is viscoelastic (Abnet and Freeman, 2000; Gu et al., 2005) and can spatially couple motion (Russell et al., 2007; Gu et al., 2005; Abnet and Freeman, 2000) suggests that it also may support waves. Shear waves along viscoelastic tissues depend on the intrinsic elasticity, density, and viscosity of the tissue (Greenleaf et al., 2003). In recent years, these kinds of waves have been demonstrated in a variety of biological tissues and the relationship between tissue material properties and waves has been well characterized (Greenleaf et al., 2003). For instance, in cancer diagnostics, the palpation of bodily tissues serves as a way to distinguish between the material properties of tumors and healthy tissues.

1.5 Thesis Goals

The primary goal of this thesis is to elucidate the functional role of the TM in hearing. To achieve this goal, I will present a novel suspended TM preparation, in which isolated TM segments were mechanically suspended between two supports in artificial endolymph bath. Using this preparation, I will mechanically stimulate the TM at audio frequencies and demonstrate a new phenomenon: longitudinally propagating

traveling waves along the TM. These waves provide insight into the dynamic material properties of the TM. More importantly, these waves have important implications for cochlear mechanics.

Second, I will apply this wave launching technique to TM segments excised from genetically modified mice that lack beta-tectorin glycoproteins. $Tectb^{-/-}$ mutant mice have previously been shown to exhibit loss of sensitivity and altered frequency tuning (Russell et al., 2007). Therefore, TM traveling waves in $Tectb^{-/-}$ mice can provide insight into the functional role of TM waves in cochlear mechanics.

Third, I will measure TM fixed charge density (c_f) using a microfabricated planar patch clamp. I will analyze the contribution of fixed charge to the mechanical properties of the TM and experimentally test whether the TM undergoes electrical-to-mechanical transduction. This study explores the mechanical role of fixed charge in the TM.

In total, the findings presented in this thesis highlight the functional significance of TM waves and the mechanical effect of fixed charge in the TM, thereby fundamentally changing the way we think about the role of the TM in cochlear function. In the short term, these findings have important implications for classical cochlear models, which must consider the consequences of longitudinally propagating traveling waves along the TM.

1.6 Document Organization

Chapters 2, 3, and 4 of this thesis have been written as paper drafts for publication and thus are intended to stand alone. Chapter 2 describes longitudinally propagating traveling waves of the TM. It was published in *Proceedings of the National Academy of Sciences, USA*. Supplemental text and figures not included in the publication are in the Appendix section of Chapter 2. In Chapter 3, I present wave measurements on TMs of mutant mice with a targeted deletion of the *Tectb* gene. In Chapter 4, I present novel microscale techniques, which I designed to measure the fixed charge density and electrokinetic properties of the TM. The final chapter (Chapter 5) broadly

summarizes all of the findings and describes the implications of the research presented in this thesis.

1.7 Direction Conventions and Nomenclature

The following coordinate system sign convention and naming will be used throughout this thesis:

Radial: Extends from the spiral limbus to the marginal band of the TM. The positive direction is towards the marginal band.

Longitudinal: Extends from the base to the apex of the cochlea. Positive direction is towards the apical end.

Transverse: Direction normal to the surface of the BM and the TM. The positive direction is towards the scala media.

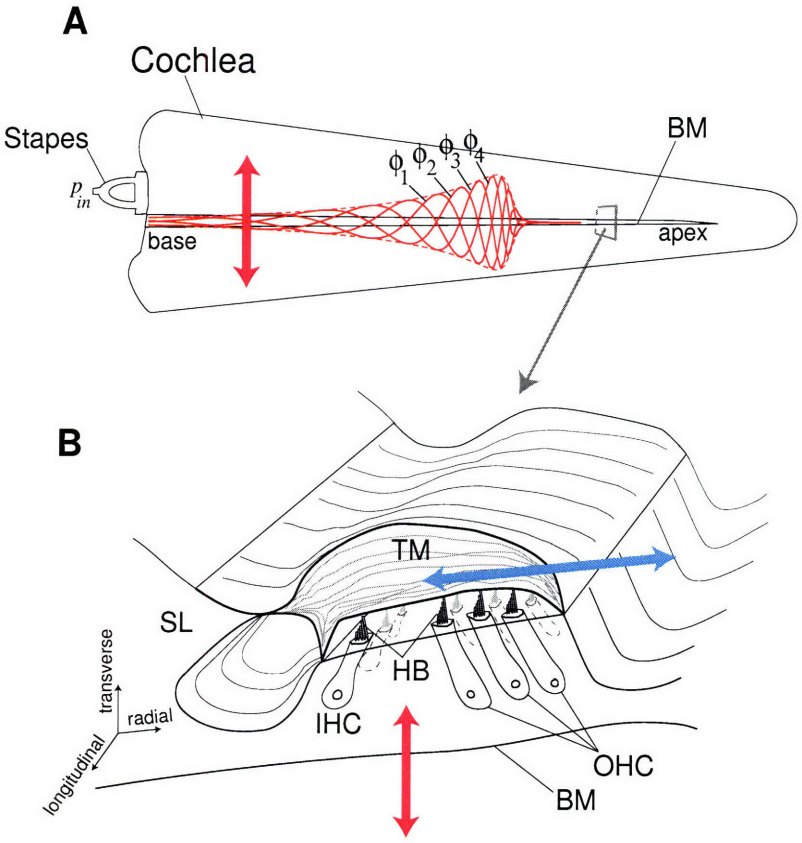

Figure 1-3: (A) Schematic drawing of mammalian cochlea showing snapshots of the BM traveling wave propagating from the base to the apex (not to scale). (B) Transverse displacements of the BM (red) are believed to generate radial shear (blue) between the TM and the apical surface of the OHCs and IHCs, which in turn causes the deflection of the hair bundles (HB).

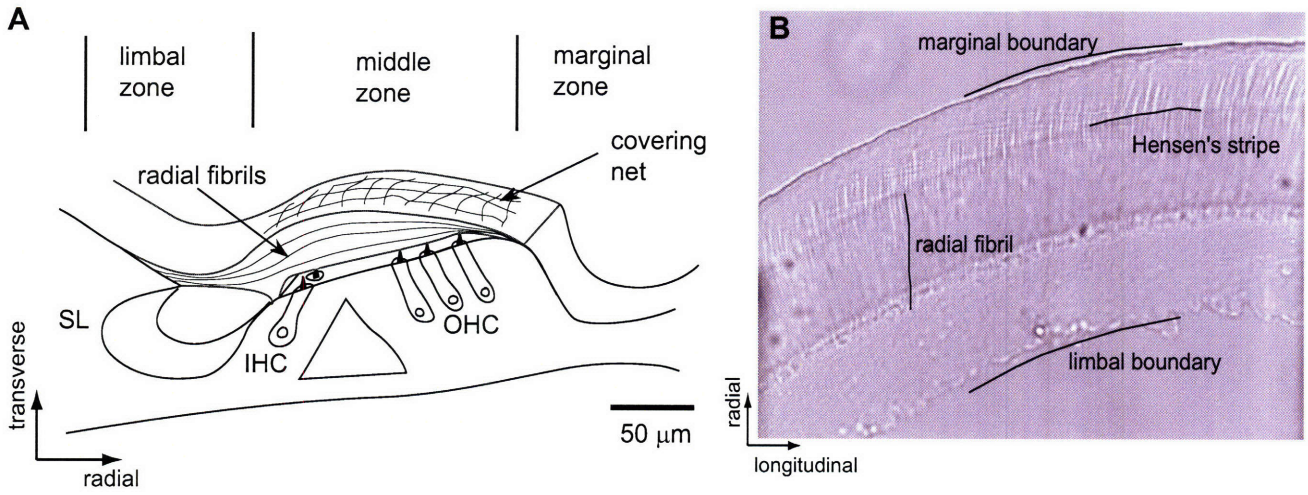

Figure 1-4: Left: The limbal zone of the TM is attached to the spiral limbus (SL). The middle and marginal zones of the TM overlie the apical surface of the hair cells. The OHC bundles are attached to the undersurface of the TM along its middle zone. The IHCs are coupled to the TM through the fluid in the subtectorial space. Right: Light micrograph of isolated TM segment excised from the base of the cochlea. Radial fibrils, Hensen's stripe, and the marginal and limbal boundaries are denoted in the image.

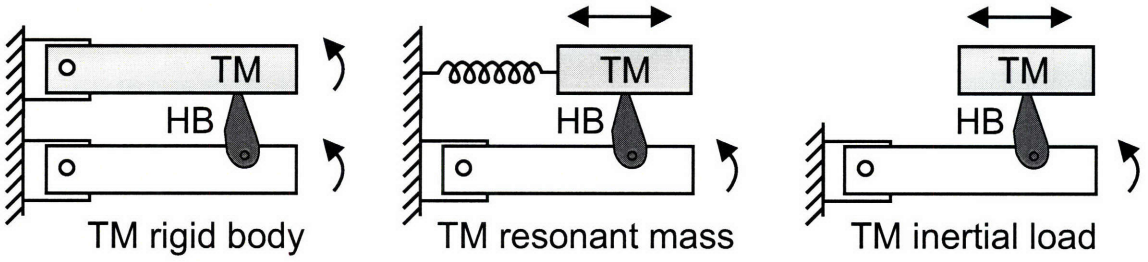

Figure 1-5: The TM has been modeled as a stiff lever (Davis, 1958; Johnstone and Johnstone, 1966; Billone and Raynor, 1973; Neely and Kim, 1983), a resonant system (Zwislocki and Kletsky, 1980; Allen, 1980; Neely and Kim, 1986), and as a pure inertial load (Mammano and Nobili, 1993) on top of the hair bundles in previous two-dimensional cross-sectional models of the cochlea. (Adapted from (Abnet, 1998)).

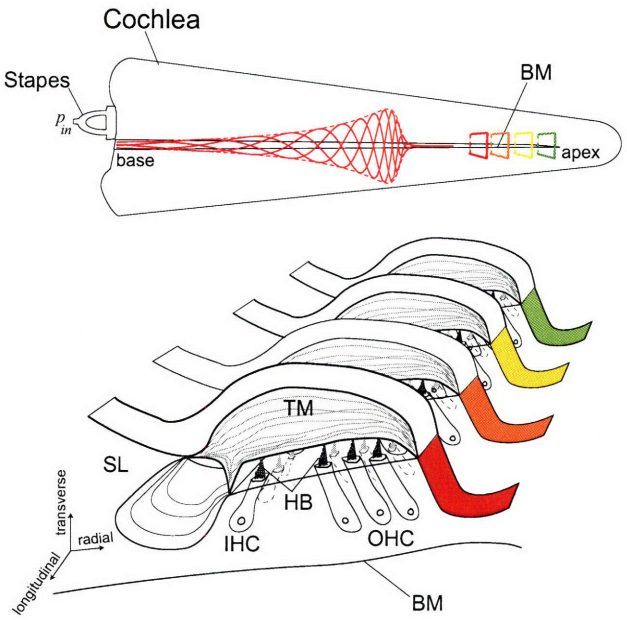

Figure 1-6: Classical models of the cochlea have assumed that adjacent structures along the cochlea are uncoupled so that radial cross-sections of the cochlear partition (color-labelled) vibrate in the radial direction independently of each other. In these models, longitudinal coupling has been assumed to occur only through the fluid in the cochlea.

Chapter 2

Longitudinally Propagating Traveling Waves of the Mammalian Tectorial Membrane

This chapter has been published in the *Proceedings of the National Academy of Sciences, USA*. The co-authors on this paper are Alexander J. Aranyosi and Dennis M. Freeman.

Abstract

Sound-evoked vibrations transmitted into the mammalian cochlea produce traveling waves that provide the mechanical tuning necessary for spectral decomposition of sound. These traveling waves of motion that have been observed to propagate longitudinally along the basilar membrane (BM) ultimately stimulate the mechanosensory receptors. The tectorial membrane (TM) plays a key role in this process, but its mechanical function remains unclear. Here we show that the TM supports traveling waves that are an intrinsic feature of its visco-elastic structure. Radial forces applied at audio frequencies (2-20 kHz) to isolated TM segments generate longitudinally propagating waves on the TM with velocities similar to those of the BM traveling wave near its best frequency (BF) place. We compute the dynamic shear

storage modulus and shear viscosity of the TM from the propagation velocity of the waves and show that segments of the TM from the basal turn are stiffer than apical segments. Analysis of loading effects of hair bundle stiffness, the limbal attachment of the TM, and viscous damping in the subtectorial space suggests that TM traveling waves can occur in vivo. Our results show the presence of a traveling wave mechanism through the TM that can functionally couple a significant longitudinal extent of the cochlea and may interact with the BM wave to greatly enhance cochlear sensitivity and tuning.

Key words: Hearing, cochlea, basilar membrane, traveling waves, tectorial membrane, longitudinal coupling.

2.1 Introduction

The mammalian cochlea is a remarkable sensor that can detect motions smaller than the diameter of a hydrogen atom and can perform high quality spectral analysis to discriminate as many as 30 frequencies in the interval of a single semi-tone (Kössl and Russell, 1995; Dallos, 1996). These extraordinary properties of the hearing organ depend on traveling waves of motion that propagate along the basilar membrane (BM) (von Békésy, 1960) and ultimately stimulate the mechano-sensory receptors. There are two types of cochlear receptors: the inner and outer hair cells. Both types of hair cells contain densely packed arrays of stereocilia called hair bundles that transduce mechanical energy into electrical signals (Hudspeth, 1985). These hair bundles project from the apical surface of hair cells towards an overlying gelatinous matrix called the tectorial membrane (TM).

The strategic anatomical configuration of the TM relative to the hair bundles suggests that the TM plays a key role in stimulating hair cells. Mouse models with genetically modified structural components of the TM have been shown to exhibit severe loss of cochlear sensitivity and altered frequency tuning (McGuirt et al., 1999; Legan et al., 2000; Simmler et al., 2000; Legan et al., 2005; Russell et al., 2007), thereby

providing further evidence that the TM is required for normal cochlear function. However, the mechanical processes by which traveling wave motion along the BM leads to hair cell stimulation remain unclear (Guinan et al., 2005), largely because the important mechanical properties of the TM have proved difficult to measure. Consequently, the mechanical function of the TM has been variously described as a rigid pivot, a resonant structure, and a free-floating mass (Davis, 1958; Zwislocki and Kletsky, 1980; Allen, 1980; Mammano and Nobili, 1993) in "classical" cochlear models, which assume that adjacent longitudinal sections of the cochlea are uncoupled except for energy propagation through the fluid (de Boer, 1997). Recent measurements have shown that the TM is visco-elastic (Abnet and Freeman, 2000) and can couple motion over significant longitudinal cochlear distances (Abnet and Freeman, 2000; Russell et al., 2007) suggesting that the TM also may support waves. Such waves have been predicted previously in the amphibian inner ear based on neurophysiological evidence (Hillery and Narins, 1984). Here we show that longitudinally propagating traveling waves are intrinsic to the dynamic material properties of the mammalian TM. The longitudinal extent of wave motion suggests that TM waves can stimulate hair cells from multiple regions of the cochlea and interact with the BM traveling wave to affect cochlear function.

2.2 Materials and Methods

2.2.1 Isolated TM Preparation

TM segments were excised from the cochleae of adult male mice (strain B6129F1, 4-10 weeks old, Taconic) using a previously published surgical technique ((Shah et al., 1995)). Additionally, TM segments were excised from the CD-1 strain of mice (4-8 weeks old, Taconic). No significant differences were found in the wave properties of TM segments excised from these two strains. In total, five B6129F1 TM segments ($n = 3$ basal and $n = 2$ apical) and six CD-1 TM segments ($n = 4$ basal and $n = 2$ apical) were studied. The cochlea was surgically removed and placed in an artificial

endolymph bath containing (in mM): 174 KCl, 5 Hepes, 3 dextrose, 2 NaCl, and 0.02 $CaCl_2$. The bath was equilibrated at pH 7.3 at room temperature. The bone casing of the cochlea was gently chipped away using a #11 scalpel blade until the organ of Corti was exposed. A combination of bright and dark-field illumination provided visual access to the TM above the organ of Corti with a dissection microscope (Zeiss). A sterilized eyelash was used to remove Reissner's membrane and to lift the TM from the cochlea. TM segments (typically 0.5-1 mm in longitudinal length) were isolated from the organ and placed in a fresh artificial endolymph bath in preparation for experiments in the wave chamber. Segments were classified as basal and apical based on the cochlear turn from which they were excised. As a secondary classification measure, we also measured the distance from the edge of the marginal band to the ridge associated with the attachment of the TM to the spiral limbus (Shah et al., 1995; Keiler and Richter, 2001). The care and use of animals in this study (NIH Grant R01 DC00238) were approved by the Massachusetts Institute of Technology Committee on Animal Care.

2.2.2 Wave Chamber

The wave chamber (Figure 2-1) consisted of two parallel supports separated by 390-480 μm. One support was attached with epoxy to a piezo-electric actuator (resonance frequency: 138 kHz, Thorlabs Inc.) and loosely coupled to the underlying glass slide. To minimize transverse motion of the actuator, the surface of the support in contact with the glass slide near the actuator was coated with a thin layer of petroleum jelly (Vaseline) in a region that was dry and isolated from fluid contact. Motion of the actuator loaded with the support and fluid was examined to ensure uniform sinusoidal motion in the radial direction. The frequency response of the vibrating system was characterized over a broad range of frequencies (1-40 kHz). The motion amplitude of the support decreased by approximately 6 dB between 1-20 kHz and exhibited a resonance at 30 kHz. TM radial displacement scaled linearly with motion of the vibrating support over the range of amplitudes (90-400 nm) applied to the TM. The second support was firmly attached to the underlying glass slide. To position a TM segment

in this experiment chamber, the surfaces of both supports were coated with 0.3 μL of tissue adhesive (Cell Tak; Collaborative Research). The tissue adhesive was dried and rinsed with ethanol resulting in a monolayer of adhesive. Artificial endolymph solution was perfused in the region of the supports and over the adhesive. The TM segment was injected into this medium with a glass-tip micropipet and suspended between the supports with a sterilized eyelash probe. The motion of the vibrating system was not affected by the attachment of the TM. The suspended region of the TM was approximately 200-300 μm above the surface of the underlying glass slide. Once the TM was successfully suspended, it was inspected for curvature. Optical sections were acquired at 0.5 μm intervals through the thickness of the TM using a light microscope coupled to a piezo-positioner (P-721 PIFOC; Physik Instrumente). The captured images rendered a three-dimensional profile of the TM and indicated a curvature of less than 2 degrees (< 6 μm) at the midpoint between the supports. TM segments were also inspected for structural damage. Segments containing tears or structural abnormalities were discarded.

2.2.3 Motion Analysis with Optical System

The optical system consisted of a 20$\times$ water immersion objective (Zeiss Axioplan) with a 0.5 numerical aperture (NA) and a transmitted light condenser (0.8 NA). Images were collected with a 12 bit, 1024$\times$1024 pixel CCD camera (CAD7-1024A, Dalsa Inc.) by strobing the light emitting diode (LED). The TM segment was illuminated at 16 evenly spaced stimulus phases over several stimulus cycles. The collected images were analyzed to determine the first 8 harmonics of the periodic motion. We computed the magnitude and phase of radial displacement from the series of collected images by using previously published motion tracking algorithms (Aranyosi and Freeman, 2004; Davis and Freeman, 1998). Radial displacement and phase were measured at multiple points along the suspended surface of the TM segment. The phase lag was measured relative to the phase at a point on the TM approximately 30 μm from the edge of the vibrating support. The experimental setup was supported by a pneumatic vibration-isolation table that damps ambient vibrations of the surround-

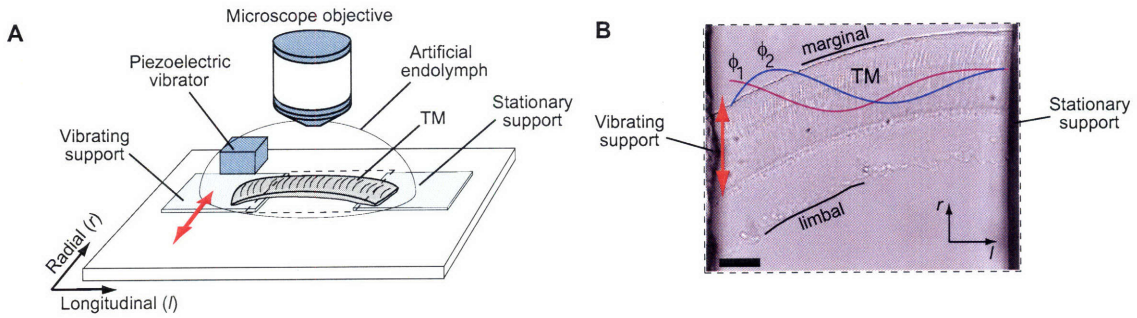

Figure 2-1: (A) Schematic of TM segment suspended between two supports (not to scale). Double-sided arrow indicates sinusoidal displacement of vibrating support at audio frequencies. Radial displacement of the TM was tracked at audio frequencies using stroboscopic illumination (see Materials and Methods). (B) Image of TM segment taken with light microscope (scale bar, 50 μm). Displacement and phase of propagating motion were tracked at several points along the TM in the region that normally overlies the hair bundles. Marginal and limbal boundaries of the TM are indicated. The two schematic waveforms pasted on the image are displacement snapshots at sequential instants (ϕ_1, ϕ_2) illustrating typical TM deformations. Displacement amplitudes were exaggerated to show the wave-like nature of the motion.

ings. Displacements at the stationary support were used to evaluate the amount of ambient noise and motion error in the measurement system. The noise floor of the measurement system was approximately 15 nm.

2.3 Results and Discussion

To study wave propagation in the TM, we developed an experiment chamber in which a segment of an isolated TM from the mouse cochlea is suspended between two parallel-aligned supports in artificial endolymph (Figure 2-1A). Sinusoidal forces applied in the radial direction at one support launched waves that propagated lon-

gitudinally along the TM toward the other support (Figure 2-1B). TM waves were bidirectional; attaching either the basal or apical end of the TM to the vibrating support launched waves. These waves were generated with nanometer-scale amplitudes (90-400 nm) over a broad range of frequencies (2-20 kHz). An optical imaging system synchronous with the driving stimulus (Aranyosi and Freeman, 2004) tracked radial displacement amplitude and phase at multiple points on the surface of the TM (see Materials and Methods).

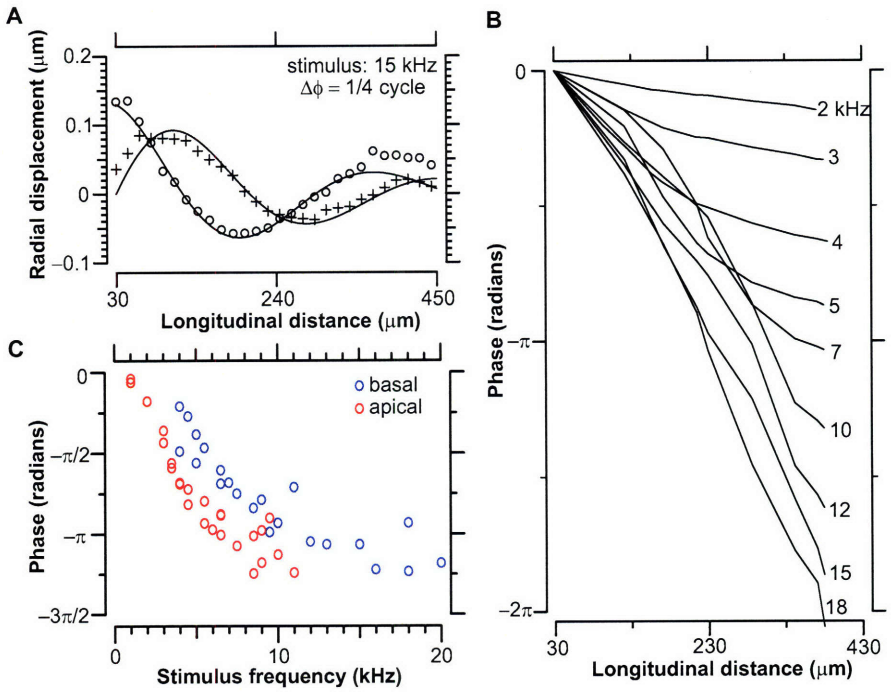

Figure 2-2: (A) TM radial displacement vs. longitudinal distance in response to 15 kHz stimulation. Radial displacement (r) is plotted as a function of longitudinal distance (x) at two instants separated by 1/4 cycle for a TM segment from the upper basal turn. Solid lines represent the equation: $r = 0.13e^{-(x-30)/237}\cos(2\pi(x\text{-}30)/350\text{-}\theta)$, with x and r in micrometers and $\theta = 0,\ \pi/2$ radians. Longitudinal distance was measured relative to a point on the TM approximately 30 μm from the edge of vibrating support. (B) Phase vs. longitudinal distance for stimulus frequencies 2-18 kHz of the basal TM segment from (A). Phase is plotted relative to 30 μm point on the TM. Phases decreased monotonically with distance and became steeper with increasing frequency. (C) Phase vs. stimulus frequency at a location on the surface of the TM approximately 250 μm from vibrating support. Each symbol represents phase lag measured relative to 30 μm point on the TM. Apical TMs (red; $n = 25$ measurements) accumulated more phase lag than basal (blue; $n = 22$ measurements) TMs at a given stimulus frequency. The entire data set represents measurements across six TM preparations (three basal and three apical TMs).

2.3.1 Longitudinal Pattern of TM Radial Motion

Figure 2-2A shows the spatial pattern of radial displacement of a typical basal TM segment in response to 15 kHz motion of one support. The two waveforms show radial displacement as a function of longitudinal distance at two instants of time separated by 1/4 cycle. An exponentially decaying sinusoid was fit to each waveform. These fits indicate wave motion of the TM. The wave has a wavelength of 350 μm and the amplitude decays with a space constant of 237 μm. The wavelength did not vary with displacement of the vibrating support. Moreover, radial displacement along the TM scaled linearly with displacement of the support.

The phase of radial displacement varied with longitudinal distance in a frequency-dependent manner. In Figure 2-2B, the phase lag at low frequencies (2 kHz) reached $\pi/6$ radians over the length of the suspended TM. In contrast, at high frequencies ($>$ 18 kHz), the phase lag exceeded a complete cycle ($> 2\pi$ radians). Phase was also measured as a function of stimulus frequency at a location on the surface of the TM approximately 250 μm from the vibrating support. Figure 2-2C shows that phase lag increased with stimulus frequency. This trend was evident across all TM samples, and the lag was larger for TM segments from the apical turn of the cochlea than for segments from the basal turn.

2.3.2 Waves Intrinsic to Dynamic Material Properties of the TM

The velocity of wave propagation (v_s) was computed as the product of frequency and wavelength for each stimulus frequency. For pure shear waves in an infinite, isotropic, visco-elastic material, v_s, is related to the shear storage modulus (G') and the shear viscosity (η), by

$$v_s = \sqrt{\frac{2(G'^2 + \omega^2\eta^2)}{\rho(G' + \sqrt{G'^2 + \omega^2\eta^2}}} \tag{2.1}$$

where ω is the angular frequency of vibration and ρ is the density of the material (Chen et al., 2004), assumed to equal that of water. Thus we can estimate G' and η by finding those values for which equation 2.1 best fits measurements of the frequency dependence of v_s. This relationship highlights the material properties that give rise to TM waves. At low frequencies, the wave velocity is determined by the ratio of G' to ρ. At high frequencies, the relevant ratio is $\omega\eta/\rho$. Thus the density, shear modulus, and shear viscosity all contribute to wave propagation.

2.3.3 Distributed Impedance Model of the TM

Although the isolated TM can support waves, the TM is loaded *in vivo* by hair bundles and damped by fluid in the subtectorial space (Allen, 1980; Zwislocki and Kletsky, 1980). To test the effects of these loads, we analyzed a distributed impedance model of the TM. The model consisted of a longitudinally distributed series of masses (M) coupled by viscous (b) and elastic (k) elements (Figure 2-3A). The radial displacements of the TM at the supports were constrained in the model as they were in the wave chamber. Moreover, in contrast to equation 2.1, this model accounts for the finite dimensions of the TM. The value for each mass component was determined by assuming the TM had the density of water. The k and b parameters are related to the shear storage modulus and shear viscosity of the TM by $G' = kd/A_{TM}$ and $\eta = bd/A_{TM}$, where d is the length of each longitudinal section and A_{TM} is the cross-sectional area. Sinusoidal stimuli applied to one end of the TM in this model launched a traveling wave similar to those seen in the wave chamber. The model accounts for the fact that fluid adjacent to the TM moves with the TM in a frequency-dependent fluid boundary layer. Fluid velocity in this layer can be approximated by

$$U(y,\omega) = U_{TM}e^{-y\sqrt{\frac{j\omega\rho}{\mu}}} \tag{2.2}$$

where ω is the radial frequency, U_{TM} is the velocity of the TM, y is the height above the TM, and ρ and μ are fluid density and viscosity, respectively (Freeman and Weiss, 1990). This fluid layer significantly increases the effective mass of the TM

and causes some damping (b_{bl}). The best fit of the model to the measurements of a typical TM segment from the upper basal turn is shown in Figure 2-3B.

Estimates of TM material properties from the distributed impedance model vary with longitudinal cochlear position. The mean values of the shear storage modulus, G', for basal and apical TM segments were 47±12 kPa ($n = 5$ TM preparations) and 17±5 kPa ($n = 3$ TM preparations), respectively. The ranges denote the standard deviation from the mean. The greater G' values of basal TMs indicates that portions of the TM from the basal turn are stiffer than those from the apical turn, as has been reported by others (Masaki et al., 2006; Gueta et al., 2006; Richter et al., 2007). Moreover, the range of G' values in the present study is somewhat larger than previous estimates of this property (Shoelson et al., 2004; Masaki et al., 2006; Richter et al., 2007) with one important exception. Gueta et al.'s quasi-static measurements in the base of the mouse cochlea (Gueta et al., 2006) are significantly larger than any other reported values. It is difficult to make comparisons of G' across studies because the TM is anisotropic (Abnet and Freeman, 2000) and the methods are different: we provide a radial stimulus that generates shear waves while others (Shoelson et al., 2004; Gueta et al., 2006; Richter et al., 2007) analyze transverse point indentations. Furthermore, these previous measurements were made at static or near static (1-10 Hz) conditions (Shoelson et al., 2004; Masaki et al., 2006; Gueta et al., 2006; Richter et al., 2007) and the mechanical properties of the TM vary with frequency (Abnet and Freeman, 2000). Thus a meaningful comparison with previous measurements requires development of a theoretical framework for comparing quasi-static and audio frequency results. The mean values of TM shear viscosity, η, ranged from 0.11 to 0.26 Pa·s, which is much greater than the viscosity of water (0.001 Pa·s). These large values of shear viscosity could result because the porous network of TM macromolecules resists the flow of interstitial fluid or because of proteoglycan interactions. Although the mean values of η were greater in basal TM segments (0.19±0.07 Pa·s) than in apical segments (0.15±0.04 Pa·s), the large ranges preclude any strong conclusions about longitudinal trends. To predict the effects of hair bundle stiffness and viscous damping in the subtectorial space, a spring (k_{hb}) representing hair bun-

dles and a dashpot (b_{sts}) representing fluid damping were added between each mass and ground (Figure 2-3A). We assumed that a nominal hair bundle stiffness of 3.5 mN/m (Kennedy et al., 2005) was evenly distributed across an 8 μm extent of the TM for each of the three rows of outer hair cells (OHCs). Adding hair bundle stiffness to the model increased space constants by $\sim$ 1%. Damping in the subtectorial space, bsts, was estimated assuming that fluid flow was Couette, so that

$$b_{sts} = \frac{\mu A_{sts}}{\delta} \tag{2.3}$$

where μ is the viscosity of the fluid in the space and A_{sts} is the cross-sectional area of each TM section facing the subtectorial space. The height of the subtectorial space, δ, was taken to be 1-6 μm based on the lengths of OHC stereocilia (Lim, 1980). Although the TM has a large intrinsic damping, viscous damping in the subtectorial space still has some frequency-dependent effects on wave motion at the narrowest gaps ($\delta = 1$ μm). In response to 7 kHz stimuli, the space constants of wave motion of a typical basal TM decreased by $\sim$ 50%. At 10 kHz, the space constants were reduced by $\sim$ 25%. These reductions in the space constants were only evident for $\delta = 1$ μm and insignificant for $\delta > 2$ μm. This suggests that subtectorial damping would have a significant effect on TM wave propagation at low frequencies only for the narrowest gaps, which occur in the extreme base of the cochlea (Lim, 1980). Since the base of the cochlea responds to high frequencies, damping in the subtectorial space does not significantly affect wave propagation near the best frequencies (BFs) of basal cochlear locations. An additional effect of including the subtectorial space in the model was to reduce the effective mass of the TM, since the subtectorial space replaced the lower fluid boundary layer. This reduction in mass caused an increase in wavelengths particularly at low frequencies. In response to 7 kHz and 10 kHz stimuli, the wavelengths were increased by $\sim$ 15% and $\sim$ 10%, respectively. Therefore, replacing the lower boundary layer with the subtectorial space increased wavelengths because of the reduced effective mass of the TM.

There is little agreement on the mechanical properties of the thin attachment of

the TM to the spiral limbus. Models of this region of the TM have ranged from completely rigid to mechanically inconsequential (Abnet and Freeman, 2000). Although there is a lack of experimental evidence to support either claim, evidence of TM radial motion in the intact cochlea (Gummer et al., 1996) suggests that the limbal attachment does not preclude TM waves. We analyzed the effects of an elastic limbal attachment by adding a spring (k_{sl}) between each mass and ground (Figure 2-3A). For sufficiently large values of k_{sl}, the limbal attachment increased the space constant and wavelength of the TM wave at low and intermediate frequencies. The model ultimately demonstrates that TM inertia, damping, and elasticity, which are comparable to those of the entire cochlear partition (Freeman, Abnet, Hemmert, Tsai and Weiss, 2003; Chan and Hudspeth, 2005b), allow TM waves to propagate even in the presence of the loads imposed by fluid in the subtectorial space, the hair bundles, and the limbal attachment.

2.3.4 Frequency Dependence of Wave Propagation Velocity

The average dimensions and typical values of G' and η for basal ($G' = 40$ kPa; $\eta = 0.33$ Pa·s) and apical ($G' = 16$ kPa; $\eta = 0.18$ Pa·s) TMs were applied in the model to compute the frequency dependence of wave propagation velocity, v_s. The measurements of v_s across basal ($n = 7$ TM preparations) and apical (n = 4 TM preparations) TMs were fit by the model predictions (Figure 2-4). The model curves and measurements have two distinct regions at low frequencies - an asymptote to infinity and a local minimum - that were dominated by the effects of the stationary support rather than by the material properties of the TM. At frequencies < 6 kHz for basal TMs and < 4 kHz for apical TMs, the wavelengths of TM waves were significantly greater than the distance between the supports. Consequently, the phase lag at low frequencies approached zero, which in turn caused v_s to increase asymptotically to larger values (Figure 2-4). The local minima were likely caused by wave reflections about the stationary support. Wave reflections can interfere with forward propagating waves and thereby reduce the effective wave propagation velocity in the forward direction. We tested these features by increasing the distance between the boundaries in the model.

This change in distance shifted the asymptotes and minima to lower frequencies, consistent with the concept that the stationary boundary increases v_s and generates wave reflections at low frequencies.

2.3.5 Wave Propagation Not Driven By Fluid Motion

Since the vibrating support drives the surrounding fluid as well as the TM in the wave chamber, we must consider the possibility that the TM is entrained to the fluid, and the observed waves are in fact fluid waves. Fluid motion decreases with increasing distance from the vibrating support, and the space constant for this decrease is the boundary layer thickness. In a two-dimensional approximation of this experimental setup (i.e., fluid velocity does not vary in the direction orthogonal to the plane of focus), the boundary layer thickness is on the order of 10 μm at 15 kHz (Freeman and Weiss, 1985). This distance is small compared to the space constant of TM wave motion ($\sim$ 240 μm) measured at 15 kHz, and energy dissipation in the third dimension will make it even smaller. Therefore, the contribution of fluid coupling to TM traveling waves is negligible compared to the effect of the intrinsic properties of the TM.

2.3.6 Longitudinal Spread of Excitation via TM Traveling Waves

The waves reported in this study suggest that significant longitudinal spread of excitation occurs via the TM (Russell et al., 2007; Zwislocki and Kletsky, 1979). The distributed impedance model (Figure 2-3) provides support for this claim by showing that TM waves are robust enough to overcome viscous dissipation in the subtectorial fluid and are sufficient to excite motions of the hair bundles. TM waves therefore provide a mechanism for extensive longitudinal coupling through cochlear structures. This finding counters a fundamental assumption made in classical cochlear models: that adjacent longitudinal sections of the cochlea are uncoupled (de Boer, 1997; Patuzzi, 1996; de Boer, 1996). The space constant measurements

at 15 kHz (Figure 2-2A) indicate that TM wave motion extends > 240 μm in the longitudinal direction. This value is much larger than previous estimates from TMs completely attached on one surface to a glass slide (Abnet and Freeman, 2000), suggesting that the attachment conditions in the previous studies significantly reduced space constants. The large spatial extent of TM wave motion is sufficient to stimulate as many as 30 rows of hair bundles, thereby coupling the activity of hair cells from multiple regions of the cochlea.

2.3.7 Effect of OHC Motility Mechanisms on TM Waves

Although we have described TM traveling waves as stimulating hair cells, it is equally plausible that these waves can arise from electromotility of OHCs (Kennedy et al., 2005; Brownell et al., 1985; Chan and Hudspeth, 2005a; Jia and He, 2005; Jia et al., 2005; Kennedy et al., 2006). Jia et al. recently reported that OHC motility generates radial motion of the TM in the hemicochlea (Jia and He, 2005; Jia et al., 2005). This finding suggests that force generation by multiple rows of OHCs via somatic motility or hair bundle motility may well be the natural driving force along the radial direction that excites longitudinally propagating waves of the TM. The physical attachment of the undersurface of the TM to the OHC hair bundles (Lim, 1980) provides further support that OHC motility can generate radial motion of the TM at multiple points along its surface, in a manner that is similar to how waves were launched in the wave chamber (Figure 2-1). In contrast to the OHC hair bundles, the inner hair cell (IHC) hair bundles are not in direct contact with the TM, but are coupled to the TM through viscous forces from the subtectorial fluid. Recent measurements using electrical stimulation across isolated turns of the guinea pig cochlea indicate that OHC motility drives radial motion of fluid in the subtectorial space (Nowotny and Gummer, 2006). This fluid flow is thought to stimulate the IHC hair bundles at frequencies below 3 kHz. Since OHC motility also drives radial motion of the TM (Jia and He, 2005; Jia et al., 2005), TM waves are likely to provide the coupling that allows OHC motility to enhance the mechanical input to IHCs (Legan et al., 2000; Jia and He, 2005; Jia et al., 2005; Nowotny and Gummer, 2006; Fridberger et al., 2006).

2.3.8 Implications for Cochlear Mechanics

The fact that TM traveling waves occur in vitro is not surprising considering that waves can be excited in a variety of elastic biological tissues (Greenleaf et al., 2003). What is striking is that TM traveling waves have large space constants and propagate with velocities (2-10 m/s) (Figure 2-4) that are comparable to the BM traveling wave near the best frequency (BF) location in response to BF stimuli (Robles and Ruggero, 2001). Therefore, the velocities of these two independent wave mechanisms can be matched near the BF location and are likely to be coupled through the OHCs, which exhibit active movements in the radial and transverse cochlear directions (Kennedy et al., 2005; Brownell et al., 1985; Chan and Hudspeth, 2005a; Jia and He, 2005; Jia et al., 2005; Kennedy et al., 2006). This type of interaction suggests that radial motion of the TM wave excites the OHC hair bundles and drives their active mechanism, which can amplify transverse motion of the BM wave. The contribution of TM waves to amplification is expected to be significant only in the region where the two waves have comparable velocities and are likely to be out of phase with respect to each other. The spatial extent of this region is likely to correspond to frequencies within approximately an octave of the BF (Rhode and Recio, 2000). The concept that the mammalian cochlea supports two traveling waves with similar propagation velocities over a limited spatial region has been suggested in a previous cochlear model (Hubbard, 1993), where the combination of the two waves was shown to produce sharp tuning and emissions.

2.3.9 Relation to TM Resonance

The fact that the TM and BM waves have similar velocities and wavelengths has important implications for the concept of TM resonance (Allen, 1980; Zwislocki and Kletsky, 1980). Previous measurements of TM and BM relative vibrations in the guinea pig cochlea have supported the idea that the TM and hair bundles behave as a resonant system (Gummer et al., 1996). This type of resonance is believed to arise from the mass of the TM and the compliance of the OHC hair bundles at frequencies

0.5 octave below the characteristic frequency (CF) of the BM (Zwislocki and Kletsky, 1980; Gummer et al., 1996). However, the effects of the TM are analyzed based on the concept of point impedance and are supported by point measurements, both of which ignore longitudinal coupling. Our measurements demonstrate that longitudinal coupling through the TM cannot be ignored and suggest that the phenomenon of TM resonance could be interpreted as a single-point simplification of a propagating TM wave.

2.4 Conclusions

We have demonstrated that radial displacements of an isolated TM excite waves of motion that propagate longitudinally with velocities similar to those of the BM traveling wave. Analysis of physiological loading effects of the hair bundles, the limbal attachment of the TM, and fluid viscosity in the subtectorial space suggests that TM waves can also propagate in vivo. Because these waves can stimulate hair cells and interact with the BM traveling wave they constitute a distinct mode of motion (Guinan et al., 2005; Mountain and Cody, 1999) that can have a significant effect on cochlear tuning and sensitivity, thereby fundamentally changing the way we think about cochlear mechanisms.

2.5 Acknowledgments

We thank C. Shera, J. J. Guinan, A. J. Grodzinsky and the members of the Cochlear Micromechanics group for helpful discussions and comments on the manuscript. We thank C. Liu and W. T. Freeman for their motion magnification algorithms. This research was supported by grant R01-DC00238 from the National Institutes of Health. R.G. was supported by a training grant from the National Institutes of Health to the Speech and Hearing Bioscience and Technology Program in the Harvard-MIT Division of Health Sciences and Technology.

2.6 Appendix

The Appendix section contains supplementary methods, results, and a comparison of TM waves to the classical BM traveling wave. The contents of this section were not included in the paper submission to PNAS. Nonetheless, this section provides further insight into how astonishingly similar TM wave properties (spatial extent, velocities, and wavelengths) are to those of the BM wave.

2.6.1 Additional Methods

Wave Chamber

The wave chamber is a novel experimental setup strategically designed for studying the dynamic material properties of the TM. The chamber suspended the TM between two supports such that a significant section of the TM was free-floating in fluid. This configuration allowed for large regions of the TM (~400-500 μm) (Figure 2-5) to remain mechanically unconstrained, thereby enabling the study of spatial coupling and wave propagation.

Suspending the TM between the supports without causing damage or tears was the most difficult task in this experiment. However, once the TM was suspended between the supports, experiments were conducted over the course of 1-3 hours. Cell-Tak bio-adhesive was used to attach the TM to the supports. The adhesion strength of Cell-Tak lasted for several hours, providing a stable environment for experiments on TM segments.

The wave chamber was designed to be compatible with various types of perfusion systems that use syringe pumps and tubing. The fluid reservoir that surrounds the suspended TM was easily accessible and could be exchanged without damaging the TM. Therefore, an implementation of a fluid inlet and outlet system is fairly straightforward in future designs of this chamber.

Other Applications of Suspended TM Experimental Setup

The fact that we can suspend the TM between supports has important implications for previous (Shoelson et al., 2004; Masaki et al., 2006; Gueta et al., 2006) and future directions in TM research. Shoelson et. al. and Gueta et. al. both extrapolated material properties from point indentations, while Masaki et. al. measured the stress-strain relation of the TM. In all of these studies, the TM was constrained on an entire surface. This attachment was assumed to be unimportant based on an underlying premise that indentations and displacements generated at the unconstrained surface of the TM did not couple motion through the entire thickness of the TM.

The wave chamber provides a way to verify the primary assumption made in these previous studies: that the attachment of the TM to a glass slide (on an entire surface) does not contribute to the measured mechanical properties of the TM. Based on the wave motion results in Figure 2-2, TM waves propagate over distances ($>$ 230 μm) that are significantly larger than the thickness of the TM. These space constants indicate that the attachment conditions are important and can dampen excited motions of the TM. Therefore, the wave chamber can be used as a novel platform for point indentation and stress-strain studies.

The following sections describe features of the experimental setup, which were not extensively covered in Chapter 2.

TM Curvature in Wave Chamber

The TM is 97% water by weight and thus has a buoyancy very similar to that of water. Consequently, the suspended TM has minimal curvature along its length. We measured the amount of curvature at the midpoint of the TM between the two supports by optically sectioning the TM with 0.5 μm step sizes. We tracked salient structural features (Hensen's stripe) at multiple planes through the thickness of the TM. The captured images indicated curvature of < 6 μm, or 2° (Figure 2-5). Moreover, visual inspection of the TM revealed that structural features, like Hensen's stripe, were in focus along the entire length of the suspended TM, thereby further showing that

curvature along the lenght of the TM was minimal compared to the thickness of the TM.

Frequency Response of Wave Chamber

The unloaded piezo-electric actuator used in the wave chamber was resonant at 138 kHz (Thorlabs, Inc.). However, this piezo actuator was coupled to a support in fluid. These additional loads can significantly alter the frequency response of the actuator. To estimate the frequency response of the actuator-support system, radial displacement of the vibrating support was measured across multiple frequencies. The frequency response of the actuator-support system had a resonance at ~30 kHz and a rapid drop-off between 30-40 kHz. The response was mostly flat between 1-20 kHz (Figure 2-6). Attaching the TM to the supports did not affect the frequency response of the wave chamber.

Launching Waves with a Microfabricated Probe

In addition to the wave chamber, TM waves were also generated with a microfabricated probe. The probe contacted the surface of the TM in the middle zone and applied shear forces in the radial direction. A large number of probes were microfabricated in polysilicon using the MUMPs process (MEMSCAP, North Carolina). Each microfabricated probe was coupled to the sharp point of a needle with epoxy. The needle was coupled at its base to a piezo-electric actuator (Thorlabs Inc), which received electrical driving signals from a computer.

TM radial displacement amplitude and phase were generated and measured at multiple points along the surface of the TM. Displacements were quantified using a previously published computer vision system (Davis and Freeman, 1998; Aranyosi and Freeman, 2004) (Figure 2-7).

Video Microscopy System

The motion of the TM was imaged through a 20×, 0.5 NA water immersion objective (Zeiss) using transmitted light. Images were collected using a 12 bit CCD camera

(CA-D7-1024A, Dalsa Inc.) with 1024×1024 pixels. The light source was a green light-emitting diode (LED) (Nichia). The green LED was strobed with a 1/8 duty cycle at the frequency of the driving stimulus. The resulting images of the TM were taken at 16 evenly spaced stimulus phases. Computer vision algorithms (Horn and Weldon Jr., 1988; Davis and Freeman, 1998) quantified the amplitude and phase of radial displacement along TM segments. The motion measurement algorithms are based on the assumption that the brightness of the structure being imaged does not change during motion.

If the brightness of a given point at a given time is $E(x, y, z, t)$, and that point moves by Δx, Δy, Δz in time Δt, then

$$E(x, y, z, t) = E(x + \Delta x, y + \Delta y, z + \Delta z, t + \Delta t). \tag{2.4}$$

The first order Taylor series expansion of the right side gives

$$\frac{\partial E}{\partial x}\Delta x + \frac{\partial E}{\partial y}\Delta y + \frac{\partial E}{\partial z}\Delta z + \frac{\partial E}{\partial t}\Delta t = 0. \tag{2.5}$$

The least-squares solution to equation 2.5 over a region of the image describes the average motion of that region. Noise in the measurements was due to ambient vibrations, drift, and noise in the imaging system. The noise floor of wave chamber setup was approximately 10 nm.

2.6.2 Additional Results

Wave Chamber Linearity

Figure 2-8A shows that TM wave amplitudes scaled linearly with displacement of the vibrating support. Additionally, the slope of the phase lag vs. longitudinal distance curves did not vary with displacement amplitude of the vibrating support (Figure 2-8B).

TM Waves Launched with Microfabricated Probe

Traveling waves were generated along the TM by applying radial shear forces with a microfabricated probe. These waves were similar to those observed in the wave chamber. The phase of radial of displacement varied with longitudinal distance in a similar manner in both experiments (Figure 2-9). The fact that TM waves can be launched using two different techniques shows that TM waves are robust. Moreover, the surface area of the microfabricated probe was designed to be comparable to the surface area of 3×3 arrays of OHC hair bundles, suggesting that radial shear forces exerted by an aggregate group of hair bundles are poised to generate TM waves.

2.6.3 Waves in the cochlea

The results presented in Chapter 2 indicate that the TM supports longitudinally propagating waves. The properties of TM waves are surprisingly similar to those of the BM traveling wave. Figure 2-10 highlights these similar properties.

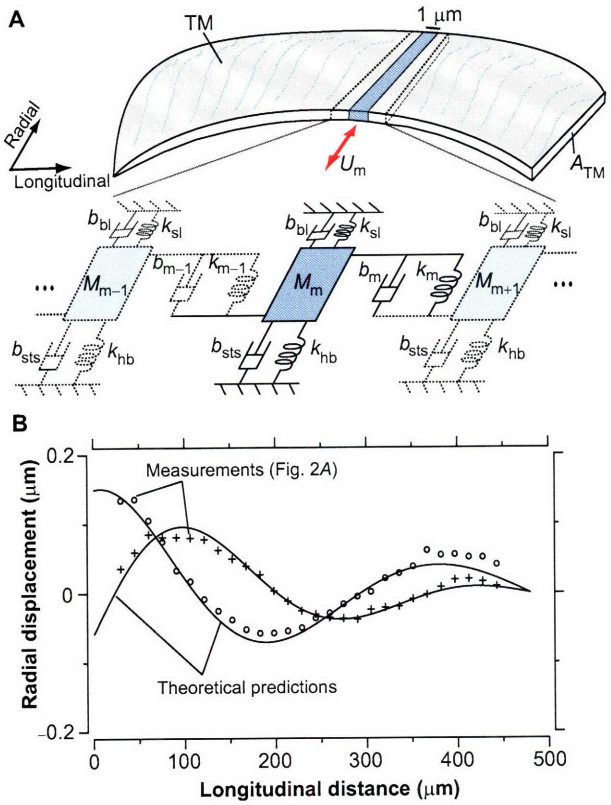

Figure 2-3: (A) (Top) Schematic highlighting a 1 μm longitudinal section (d) of the TM (dark gray) with rectangular cross-sectional area, A_{TM}. Vibrating support can generate radial motion of this TM section with velocity, U_m, through longitudinal coupling. (Bottom) Mechanical circuit representation of TM section consisting of a mass (M_m) coupled to adjacent sections (M_{m-1}, M_{m+1}) by viscous (b_m, b_{m-1}) and elastic (k_m, k_{m-1}) components. The effective mass of each TM section included the mass of the fluid layers above and below the TM. Effect of damping in the fluid layer was investigated by adding a dashpot (b_{bl}) between each mass and ground. Effects of cochlear loads: viscous damping in the subtectorial space (b_{sts}), hair bundle stiffness (k_{hb}), and the elastic effect of the limbal attachment (k_{sl}) were investigated by adding a dashpot and two springs between each mass and ground. (B) Comparison of TM wave measurements in the wave chamber to theoretical predictions of the distributed impedance model. Symbols (+, $\circ$) denote motion measurements of the upper basal TM segment from Figure 2-2A. Lines represent least-squares fits of the theoretical predictions to these experimental results. The best fit values of shear storage modulus, G', and shear viscosity, η, applied in the model across multiple frequencies for this TM were 30 kPa and 0.13 Pa·s, respectively. Velocities at the extreme longitudinal ends of the TM segment were constrained in the model as they were by the supports in the TM wave experiments.

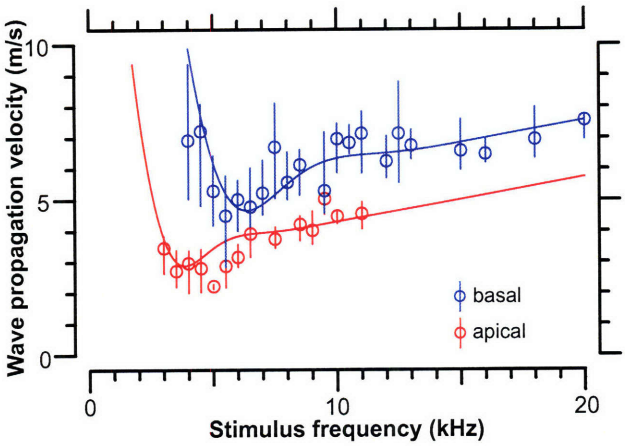

Figure 2-4: The circles represent the median values of wave propagation velocity, v_s, measured across multiple frequencies for basal ($n = 7$ TM preparations; blue) and apical ($n = 4$ TM preparations; red) segments. Interquartile ranges (IQRs) are represented with vertical lines. Lines represent model predictions of v_s versus frequency generated from the average dimensions of basal and apical TM segments and from material property estimates (G' and η) of these segments. Typical values of G' and η for basal ($G' = 40$ kPa; $\eta = 0.33$ Pa·s) and apical ($G' = 16$ kPa; $\eta = 0.18$ Pa·s) TM segments were applied to estimate the frequency dependence of v_s in the model.

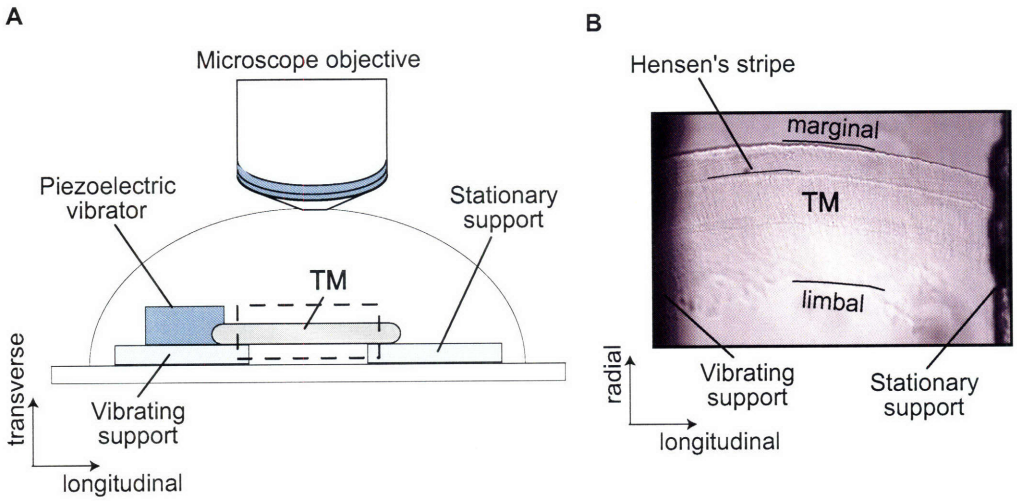

Figure 2-5: (A) Schematic of the TM in the wave chamber, illustrating the suspended region. (B) Light microscopy indicates that co-planar features of the TM, like Hensen's stripe, remained in the same plane of focus along the length of the TM.

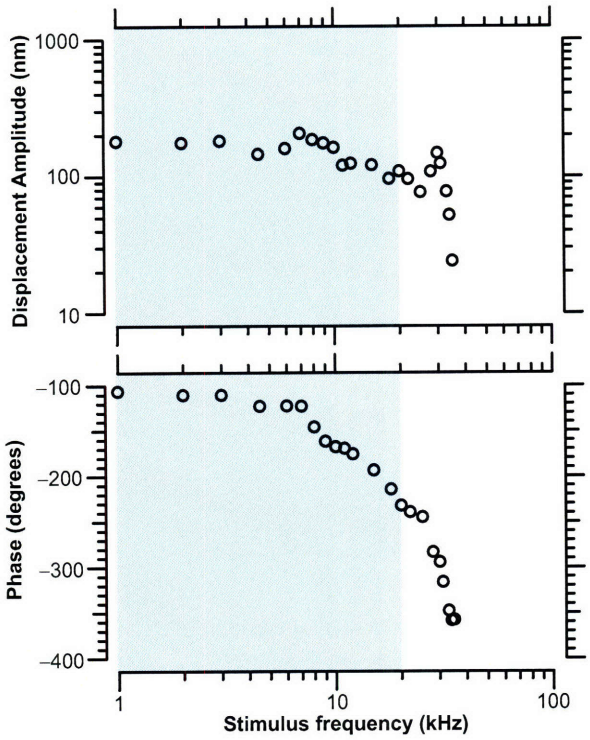

Figure 2-6: The frequency response of the piezo-driven vibrating support in fluid was roughly flat with a slight downward slope from 1 to 20 kHz. There was a resonance at $\sim$ 30 kHz followed by a rapid decrease in amplitude. The motion was decreased by approximately 6 dB over the range of stimulus frequencies applied to the TM. Shaded regions denote range of stimulus frequencies applied to the TM.

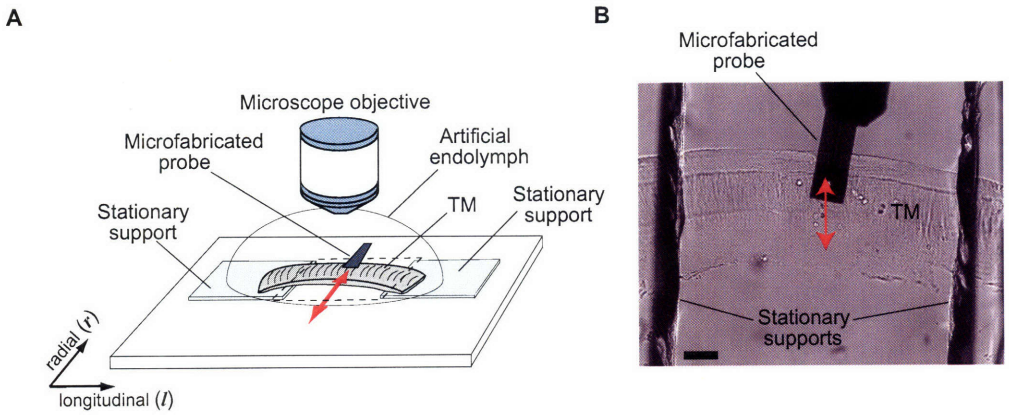

Figure 2-7: Waves were launched on the TM with microfabricated probe, which acted as a displacement source. The TM was suspended between two supports similar to the wave chamber. But instead of the vibrating support, a microfabricated probe coupled to a piezo-electric actuator was attached to the surface of the TM at the midpoint between the two supports. The contact region of the probe and the TM was typically over the middle zone of the TM. Wave motions were captured with a computer vision system as in the wave chamber experiments. Scale bar: 30 μm.

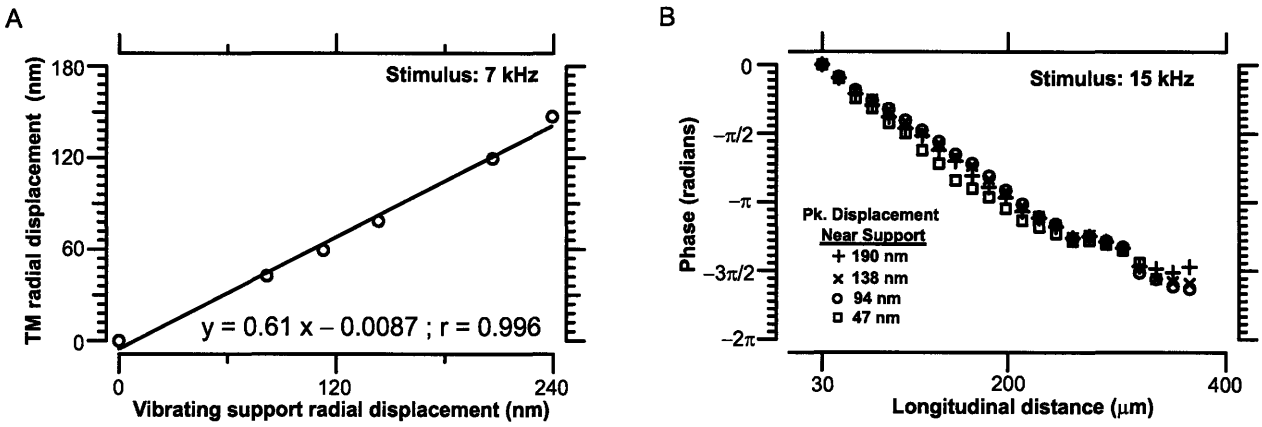

Figure 2-8: (A) TM radial displacement measured in response to 7 kHz stimulation at a location on the surface of the suspended TM $\sim$ 100 μm from the vibrating support.TM radial displacement scaled linearly with motion of the vibrating support. Line represents a linear regression fit ($r^2 = 0.992$) to the displacement data ($n = 6$) with a slope of 0.61. (B) Phase vs. longitudinal distance at 15 kHz stimulation. Phase lag was measured over range of displacement amplitudes applied to the TM. The peak displacement amplitudes were at a point on the surface of the TM $\sim$ 30 μm away from the vibrating support. Phase lag and wavelength of the TM were roughly constant over the range of displacements tested ($\sim$ 50-300 nm). The four symbols ($\times$, $\circ$, $+$, $\sqcap$) represent measurements at different displacement amplitudes applied to a basal TM segment.

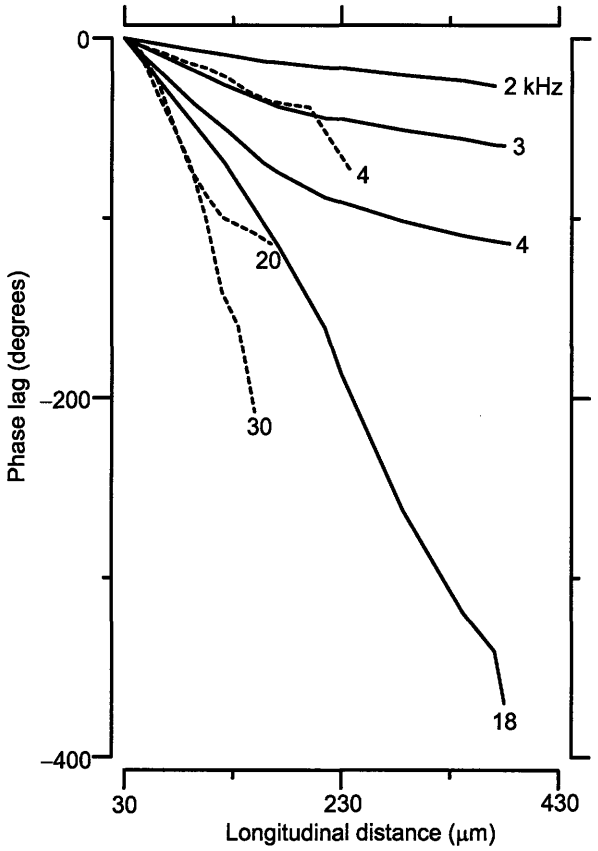

Figure 2-9: Phase lag vs. longitudinal distance was measured using two different techniques. The solid lines represent measurements in the wave chamber from Figure 2-2. The dashed lines denote phase measurements conducted with the microfabricated probe. Phase was measured relative to a point on the surface of the TM $\sim$30 μm from the stimulus source in both experiments.

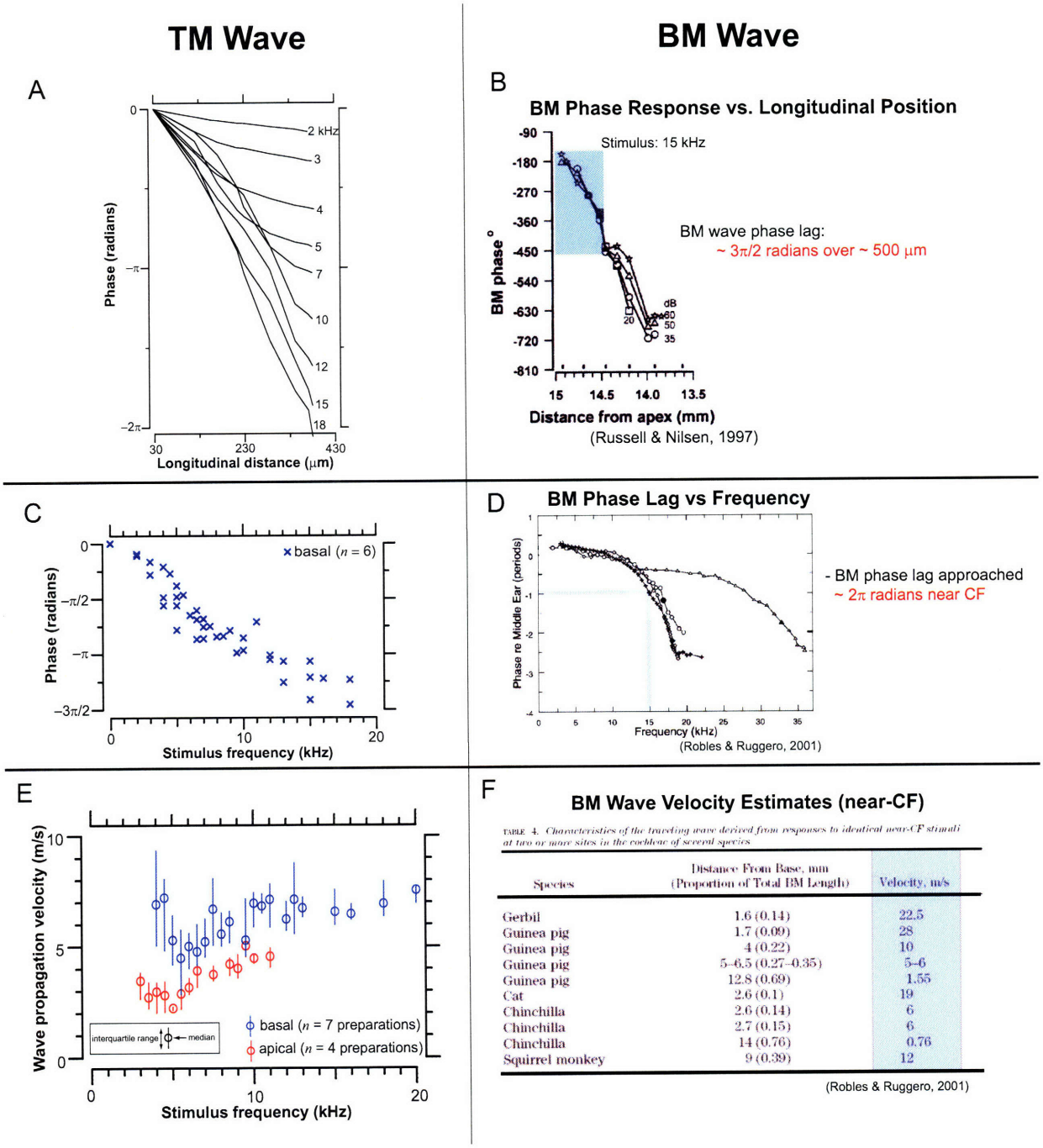

Figure 2-10: (A,B) Phase lag accumulation vs. longitudinal distance along the TM was comparable to phase lag accumulation over comparable distances along the BM (Russell and Nilsen, 1997). (C,D) Group delays near CF along TM segments were comparable to delays measured near CF for the BM wave (Robles and Ruggero, 2001). (E,F) TM wave propagation velocities were comparable to the BM wave velocities measured near the CF location (Robles and Ruggero, 2001).

Chapter 3

Longitudinally Propagating Traveling Waves in Genetically Modified Mammalian Tectorial Membranes

Abstract

It is widely believed that the extraordinary sensitivity and frequency selectivity of the mammalian cochlea depend on traveling waves of motion that propagate along the basilar membrane (BM) and ultimately stimulate the mechano-sensory receptors (von Békésy, 1960). However, new experimental evidence suggests that a gelatinous matrix called the tectorial membrane (TM) also support waves that can help stimulate these receptors (Ghaffari et al., 2007). Here we investigate longitudinally propagating traveling waves along isolated TM segments from mice with a targeted deletion of the *Tectb* gene*, which encodes beta-tectorin glycoproteins in the TM. $Tectb^{-/-}$ mutant mice have been previously shown to exhibit a significant reduction in cochlear sensitivity and sharpened tuning compared to wild types (Russell et al., 2007). We show

*We thank Guy Richardson for generously providing these mice to our group.

that the longitudinal extent and velocity of TM traveling waves are significantly reduced in $Tectb^{-/-}$ mice. The differences in TM wave properties between mutants and wild types arise from changes in the mechanical properties of the TM; mutant TMs are significantly less stiff than wild type TMs are. Therefore, slight modifications to TM structural constituents altered the mechanical properties of the TM in $Tectb^{-/-}$ mice and thereby affected wave propagation. Our results are consistent with the concept that there is a reduction in the spread of excitation via TM waves and less TM wave interaction with the BM traveling wave in $Tectb^{-/-}$ mice compared to wild types, suggesting that TM waves are crucial for sensitivity and frequency selectivity in the cochlea.

Key words: cochlear mechanics, Tectb, beta-tectorin, longitudinal coupling

3.1 Letter

Recent advancements in genetic manipulation studies of the tectorial membrane (TM) have generated a greater understanding of TM molecular biology and provided strong evidence that the TM is required for normal hearing (McGuirt et al., 1999; Legan et al., 2000; Simmler et al., 2000; Legan et al., 2005; Russell et al., 2007). What is striking about the molecular biology of the TM is the presence of unique glycoproteins. In particular, two of the three non-collagenous proteins found in the TM, alpha-tectorin and beta-tectorin, are expressed exclusively in the TM and nowhere else in the cochlea (Killick et al., 1995; Goodyear and Richardson, 2002). Consequently, the tectorins are ideal candidates for genetic modifications of the TM (Legan et al., 2000; Simmler et al., 2000; Legan et al., 2005; Russell et al., 2007). A recent study found that mice with a targeted deletion of *Tectb* (the gene that encodes beta-tectorin) exhibit an unusual phenotype: a ~50 dB SPL reduction in cochlear sensitivity at low frequencies and sharpened frequency tuning (Russell et al., 2007). The basilar membrane (BM) tuning curves in $Tectb^{-/-}$ mice ($Q_{10dB} = 18.6 \pm 2.6$) were significantly sharper than those in $Tectb^{+/+}$ mice ($Q_{10dB} = 9.6 \pm 3.3$) (Russell et al., 2007). A similar increase in

sharpness of tuning was also evident in the neural tuning data. These differences in sensitivity and frequency tuning between mutants and wild types were attributed to a reduction in the spread of excitation along the cochlea by mutant TMs. The fact that the TM supports waves suggests that TM waves can help produce this spread of excitation along the cochlea (Ghaffari et al., 2007). Therefore, any differences in hearing sensitivity and frequency tuning between mutants and wild types may be driven by changes in TM traveling wave properties.

To determine how the loss of beta-tectorin affects TM traveling waves, we investigated wave motion along TMs excised from $Tectb^{-/-}$ mutant mice. Isolated TM segments were suspended between two supports in a wave chamber as reported previously (Ghaffari et al., 2007) (see Materials and Methods). Sinusoidal forces applied in the radial direction at one support generated waves that propagated longitudinally along the TM toward the other support. These waves were nanometer-scale in amplitude and observed over a broad range of frequencies (1-20 kHz). An optical system that used stroboscopic illumination tracked displacement amplitude and phase at multiple points on the surface of the TM (Aranyosi and Freeman, 2004; Ghaffari et al., 2007).

Figure 3-1 shows the longitudinal pattern of radial displacement of typical basal and apical TM segments from $Tectb^{-/-}$ and wild type mice. Basal mutant TM segments had wavelengths that were slightly smaller than those of basal wild type TM segments (Figure 3-1A). In contrast, apical mutant TMs had wavelengths that were significantly smaller than those of apical wild type TMs (Figure 3-1B). Figure 3-2 shows that the spacial extent of TM waves also was significantly reduced in mutants compared to wild types. The wave decay constants of basal mutants were $\sim$100-150 μm ($n = 3$ TM preparations) compared to $\sim$250 μm in basal wild types ($n = 7$ TM preparations) (Figure 3-2A). The wave decay constants of apical mutant TMs were typically between 100-200 μm compared to > 300 μm in apical wild type TMs (Figure 3-2B).

The phase of radial displacement was measured as a function of stimulus frequency at a location on the surface of the TM $\sim$250 μm from the vibrating support. Figure 3-

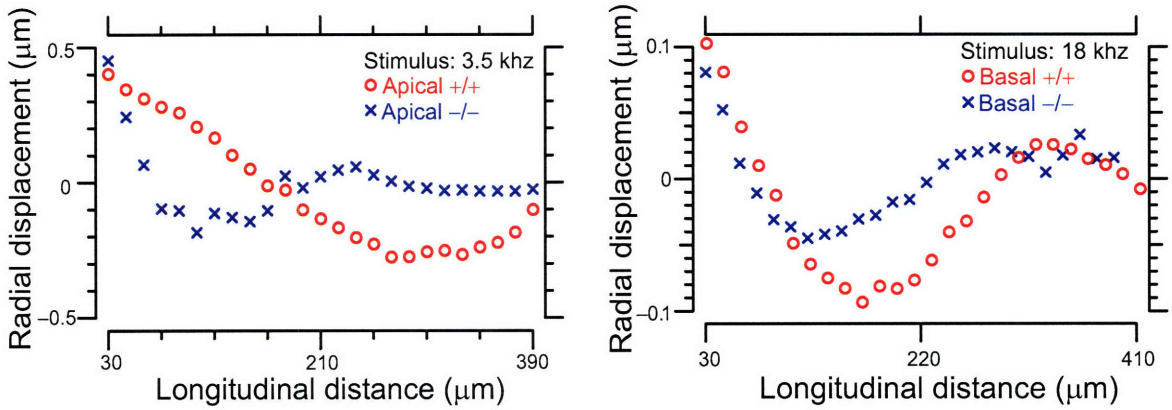

Figure 3-1: (Left) TM radial displacement vs. longitudinal distance in response to 3.5-kHz stimulation for an apical mutant TM (×) and an apical wild type TM (o). (Right) TM radial displacement vs. longitudinal distance in response to 18-kHz stimulation for a basal mutant TM (×) and a basal wild type TM (o). Longitudinal distance was measured relative to a point on the surface of TM approximately 30 μm from the edge of vibrating support. This point on the TM was designated as the 30-μm point in both plots.

3A shows that basal mutant TMs exhibited more phase lag accumulation than basal wild types. Across apical TMs, phase lag accumulation in mutants was significantly larger than the lag measured in wild types (Figure 3-3B).

The velocity of wave propagation (v_s) of mutant and wild type TMs was computed as the product of frequency and wavelength. The frequency dependence of v_s is reported in Figure 3-4. Estimates of v_s were smaller in mutants compared to wild types (Figure 3-4). Across basal TM segments, v_s median values were between 2-5 m/s in mutants compared to 4-8 m/s in wild types. In apical segments, v_s median values were between 1-2 m/s and 3-5 m/s in mutants and wild types, respectively.

For pure shear waves, the shear modulus (G'), the shear viscosity (η), and density (ρ) of a material are related to v_s (Chen et al., 2004; Ghaffari et al., 2007). A distributed impedance model of the TM (Ghaffari et al., 2007), which accounts for the finite dimensions of the TM and the mass and viscosity of the fluid in the bound-

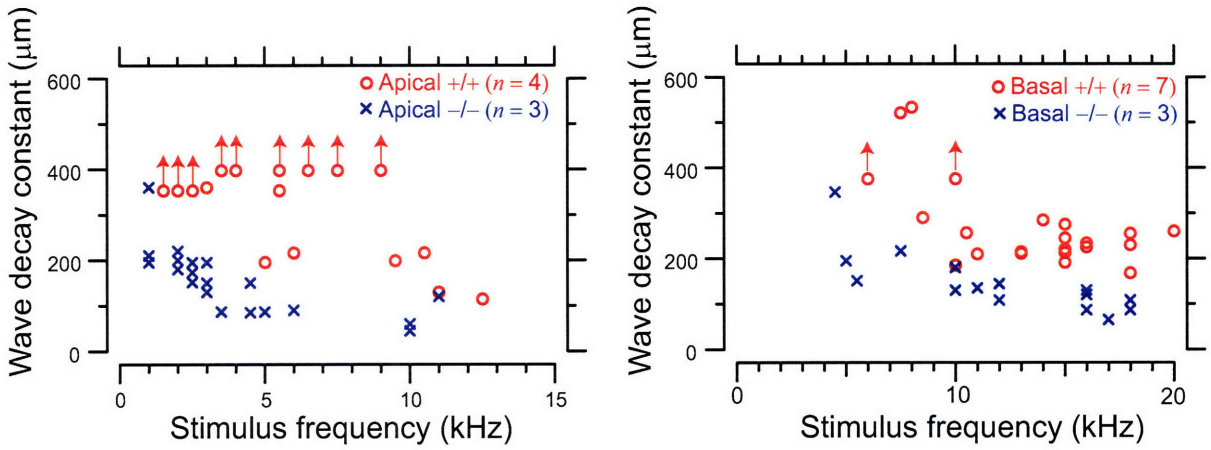

Figure 3-2: (Left) TM wave decay constants were measured across multiple frequencies in apical mutant and wild type TMs. TM waves decayed more rapidly with longitudinal distance in basal mutant TMs than in wild types. Wave decay constants tended to decrease with increasing frequency for both mutants and wild types. (B) Wave decay constants of basal mutants were significantly smaller than those of apical wild types. The upward pointing arrows denote wave decay constant values that were significantly larger than the distance between the supports.

ary layer surrounding the TM, was used to estimate the shear storage modulus, G', and the shear viscosity, η. Sinusoidal stimuli applied to one end of the TM in this model launched traveling waves along mutant TMs similar to those measured experimentally. Therefore, we can estimate the material properties (G' and η)[†] of mutant TM segments from best fits to the measurements of the frequency dependence of v_s (Figure 3-4).

Similar to wild type TMs, estimates of TM material properties in mutants varied with longitudinal cochlear position. The mean values of the shear storage modulus, G', for basal ($n = 3$ TM preparations) and apical ($n = 3$ TM preparations) mutant TMs were 7 kPa and 1 kPa, respectively. The mean values of the shear viscosity, η, for basal ($n = 3$ TM preparations) and apical ($n = 3$ TM preparations) mutant TMs

[†]The density, ρ, of the TM was assumed to be equal to that of water.

were 0.18 Pa·s and 0.10 Pa·s, respectively. These values of G' and η are significantly smaller than previous mean estimates of material properties in wild type basal ($G' =$ 40 kPa; $\eta = 0.33$ Pa·s) and apical ($G' = 16$ kPa; $\eta = 0.18$ Pa·s) TMs (Ghaffari et al., 2007), suggesting that mutant TMs are significantly less stiff and somewhat less intrinsically viscous than wild types are.

Because mutant TMs have larger volumes than wild types in the apical coil of the cochlea (Russell et al., 2007), we must consider the possibility that any differences in material and mechanical properties of the TM may be caused by differences in geometry and boundary conditions. Russell et al. reported that the thickness of mutant TMs (72.1±3.5 μm) was larger than that of wild types (36.4±1.9 μm) (Russell et al., 2007). However, the estimates of G' and η are based on a distributed impedance model, which accounts for the finite dimensions of the TM (Ghaffari et al., 2007). Therefore, the differences in wave properties are likely caused by changes in the intrinsic material properties of the TM in mutants. The findings reported in this study ultimately demonstrate that $Tectb^{-/-}$ mutant mice have TMs that are more compliant. Consequently, these TMs support waves that have significantly slower propagation velocities than wild type TMs.

The observations presented in this study have broad implications for cochlear mechanics. The most striking effects of the *Tectb* mutation was to significantly reduce sensitivity while sharpening cochlear tuning relative to wild types. This concept is counter-intuitive in light of classical cochlear models because it suggests that sensitivity and frequency tuning are somehow uncoupled.

The measurements on the longitudinal extent of mutant TM waves (Figure 3-1, Figure 3-2) are consistent with the concept that there is less spread of cochlear excitation (sharpened frequency tuning) in $Tectb^{-/-}$ mice. The longitudinal extent of TM waves was reduced by a factor of 2-4 in mutants, suggesting that fewer hair cells are stimulated by TM waves in mutants than in wild types. To compare these estimates to the frequency tuning curves reported by Russel et al. (2007), we invoked scaling symmetry and a frequency place map of the mouse cochlea (Muller et al., 2005). The bandwidth of spatial tuning curves at 20 kHz for mutants and wild types

were 220 μm and 150 μm, respectively. This 30% decrease in spread of excitation along the cochlea in mutant mice is comparable to the reduction in spatial extent of TM waves in mutants compared to wild types (~55% decrease in wave decay constants near 20 kHz).

The propagation velocity of TM waves also may have important implications for cochlear mechanics. In particular, the extent of cochlear amplification may be affected by the extent of interaction between the TM and BM traveling waves. The contribution of TM waves to cochlear amplification is expected to be significant only in the cochlear region where the two waves have matching propagation velocities near the best frequency location (Hubbard, 1993; Rhode and Recio, 2000). Since the apical TM segments of *Tectb*$^{-/-}$ mutant mice support waves with significantly reduced velocities (by up to a factor of 5) compared to wild types, it is likely that the TM and BM waves are not closely matched in the apical coil of the cochlea in mutants. The presence of two waves with unmatched velocities suggests that the TM and BM waves cannot interact, thereby leading to a significant reduction in sensitivity. This concept is consistent with there being a substantial loss of cochlear sensitivity in *Tectb*$^{-/-}$ mutant mice (~50 dB SPL) at low frequencies (Russell et al., 2007). In contrast, TM wave velocities were reduced by less than a factor of 2 in basal mutants compared to basal wild types at high frequencies. Therefore, TM and BM waves may be somewhat matched in the basal coil of the cochlea in *Tectb*$^{-/-}$ mice, consistent with there being only a slight decrease in hearing sensitivity (~10 dB SPL) at high frequencies (Russell et al., 2007). This analysis does not factor in the relative phase of the TM and BM waves, which is important for understanding how the waves may interact. Nevertheless, the fact that changes in TM wave velocities correlate with shifts in cochlear sensitivity in mutants suggests that these waves are poised to play a key role in cochlear amplification.

Our observations demonstrate that a targeted deletion of the *Tectb* gene significantly alters the wave properties of the TM. These changes in the spatial extent and velocity of mutant TM waves are consistent with the reduction in sensitivity and sharpened frequency tuning exhibited by *Tectb* mutant mice. It is important to note

that auditory function in these mutant mice are largely inconsistent with classical models of the cochlea, in which loss of sensitivity is always coupled to broadened frequency tuning. Our results fundamentally question concepts of the TM in classical cochlear models and ultimately highlight the importance of TM waves in cochlear mechanisms.

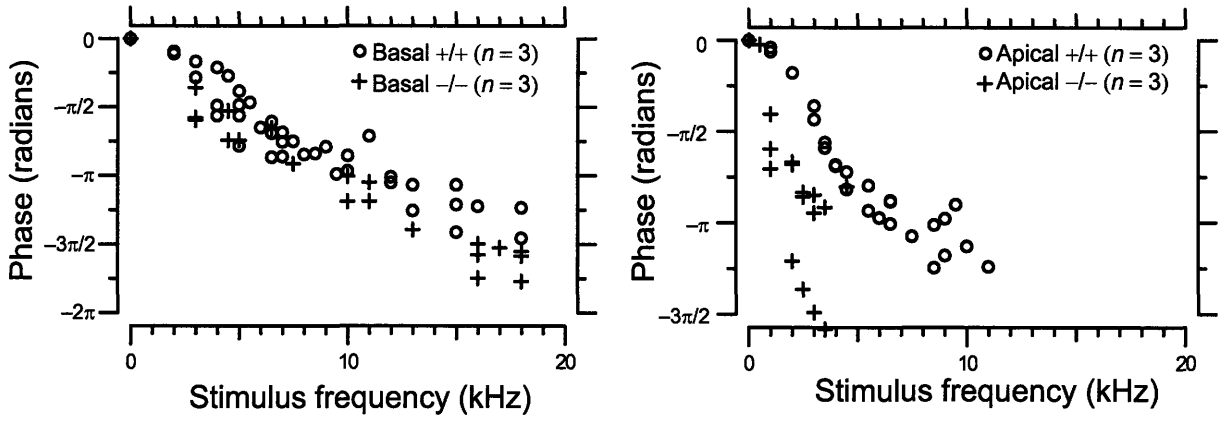

Figure 3-3: (Left) Basal mutant TM segments (n = 3 TM preparations; +) exhibited more phase lag compared to wild types (n = 3 TM preparations; o). (Right) Phase lag accumulation was significantly larger for mutant apical TMs (n = 3 TM preparations; +) compared to apical wild types (n = 3 TM preparations; o).

3.2 Materials and Methods

3.2.1 Isolated TM Preparation

TM segments were excised from the cochleae of $Tectb^{-/-}$ and $Tectb^{+/+}$ adult male mice (strain B6/129, 4-10 weeks old, Taconic) and suspended in a wave chamber using a previously published technique (Ghaffari et al., 2007). The cochlea was surgically removed and placed in an artificial endolymph bath containing (in mM): 174 KCl, 5

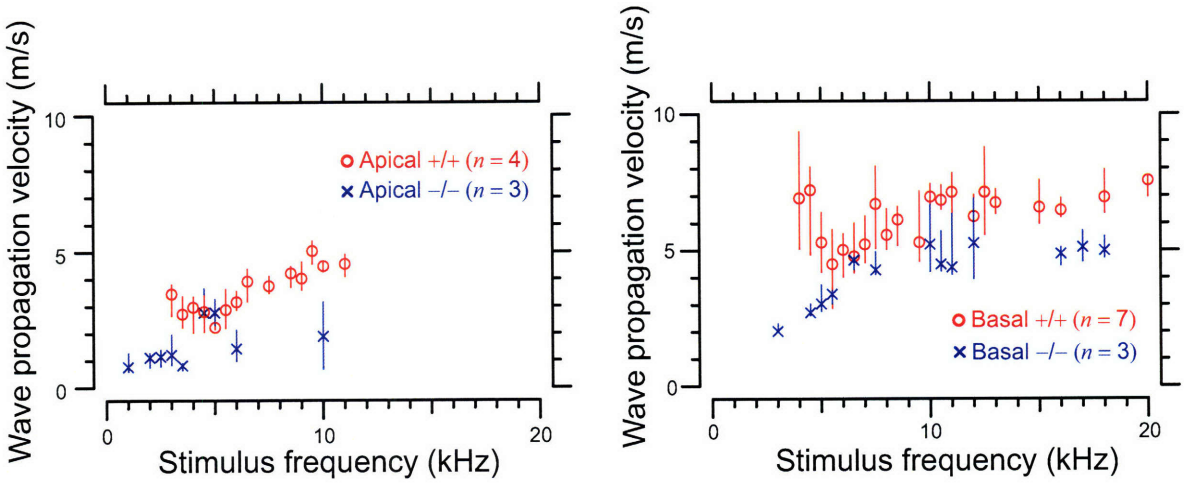

Figure 3-4: (A) Mutant apical TM segments ($n = 3$ TM preparations; $\times$) had significantly slower wave propagation velocities, v_s, values compared to apical wild types TMs ($n = 4$ TM preparations; o). (Right) Mutant basal TM segments ($n = 3$ TM preparations; $\times$) had somewhat slower wave propagation velocity, v_s, values compared to wild types ($n = 7$ TM preparations; o). Symbols represent the median values of v_s measured across multiple stimulus frequencies for basal and apical TM segments. Interquartile ranges are represented with vertical lines.

Hepes, 3 dextrose, 2 NaCl, and 0.02 $CaCl_2$. The bath was equilibrated at pH 7.3 at room temperature. The bone casing of the cochlea was gently chipped away using a #11 scalpel blade until the organ of Corti was exposed. A combination of bright and dark-field illumination provided visual access to the TM above the organ of Corti with a dissection microscope (Zeiss). A sterilized eyelash was used to remove Reissner's membrane and to lift the TM from the cochlea. TM segments (typically 0.5-1 mm in longitudinal length) were isolated from the organ and placed in a fresh artificial endolymph bath in preparation for experiments in the wave chamber. Segments were classified as basal and apical based on the cochlear turn from which they were excised. As a secondary classification measure, we also measured the distance from the edge of the marginal band to the ridge associated with the attachment of the TM to the spiral limbus (Russell et al., 2007). The care and use of animals in this study (NIH

Grant R01 DC00238) were approved by the Massachusetts Institute of Technology Committee on Animal Care.

3.2.2 Wave Chamber

The wave chamber (Figure 2-1) consisted of two parallel supports separated by 390-480 μm. One support was attached with epoxy to a piezo-electric actuator (resonance frequency: 138 kHz, Thorlabs Inc.) and loosely coupled to the underlying glass slide. To minimize transverse motion of the actuator, the surface of the support in contact with the glass slide near the actuator was coated with a thin layer of petroleum jelly (Vaseline) in a region that was dry and isolated from fluid contact. Motion of the actuator loaded with the support and fluid was examined to ensure uniform sinusoidal motion in the radial direction. The frequency response of the vibrating system was characterized over a broad range of frequencies (1-40 kHz). The motion amplitude of the support decreased by approximately 6 dB between 1-20 kHz and exhibited a resonance at 30 kHz. TM radial displacement scaled linearly with motion of the vibrating support over the range of amplitudes (90-400 nm) applied to the TM. The second support was firmly attached to the underlying glass slide. To position a TM segment in this experiment chamber, the surfaces of both supports were coated with 0.3 μL of tissue adhesive (Cell Tak; Collaborative Research). The tissue adhesive was dried and rinsed with ethanol resulting in a monolayer of adhesive. Artificial endolymph solution was perfused in the region of the supports and over the adhesive. The TM segment was injected into this medium with a glass-tip micropipet and suspended between the supports with a sterilized eyelash probe. The suspended region of the TM was approximately 200-300 μm above the surface of the underlying glass slide. Once the TM was successfully suspended, it was inspected for curvature. Optical sections were acquired at 0.5 μm intervals through the thickness of the TM using a light microscope coupled to a piezo-positioner (P-721 PIFOC; Physik Instrumente). The captured images rendered a three-dimensional profile of the TM and indicated a curvature of less than 2° (< 6 μm) at the midpoint between the supports. TM segments were also inspected for structural damage. Segments containing tears or

structural abnormalities were discarded.

3.2.3 Motion Analysis with Optical System

The optical system consisted of a 20× water immersion objective (Zeiss Axioplan) with a 0.5 numerical aperture (NA) and a transmitted light condenser (0.8 NA). Images were collected with a 12 bit, 1024×1024 pixel CCD camera (CAD7-1024A, Dalsa Inc.) by strobing the light emitting diode (LED). The TM segment was illuminated at 16 evenly spaced stimulus phases over several stimulus cycles. The collected images were analyzed to determine the first 8 harmonics of the periodic motion. We computed the magnitude and phase of radial displacement from the series of collected images by using previously published motion tracking algorithms (Aranyosi and Freeman, 2004; Davis and Freeman, 1998). Radial displacement and phase were measured at multiple points along the suspended surface of the TM segment. The phase lag was measured relative to the phase at a point on the TM approximately 30 μm from the edge of the vibrating support. The experimental setup was supported by a pneumatic vibration-isolation table that damps ambient vibrations of the surroundings. Displacements at the stationary support were used to evaluate the amount of ambient noise and motion error in the measurement system. The noise floor of the measurement system was approximately 15 nm.

3.3 Supplementary Information

3.3.1 Materials and Methods

Gene Targeting

Gene targeting in embryonic stem cells was previously used to delete specific exons of the *Tectb* gene (Russell et al., 2007). Beta-tectorin was not detected in the TM or in the organ of Corti in $Tectb^{-/-}$ mutant mice as a result of this deletion and the distribution of alpha-tectorin and otogelin were unaffected by this mutation. A detailed account of the gene targeting procedure was previously reported (Russell

et al., 2007).

Electro-Physiology Measurements

Cochlear sensitivity and frequency tuning have been previously reported in $Tectb^{-/-}$ mutant mice and wild types (Russell et al., 2007). We applied similar methods to measure distortion product otoacoustic emissions (DPOAEs) and auditory brainstem responses (ABRs) in these mice. These techniques have been described in detail previously (Maison et al., 2002). Mice were anesthetized with xylazine (20 mg/kg) and ketamine (100 mg/kg) prior to electrophysiological experiments. All experiments were conducted in a soundproof chamber.

Distortion Product Otoacoustic Emissions (DPOAEs)

DPOAEs at $2f_1$-f_2 were recorded using a custom acoustic assembly consisting of two 0.25 inch condenser microphones, used to generate two primary tones, and a Knowles miniature microphone (EK3103; Knowles Electronics, Franklin Park, IL), which recorded sound pressure in the ear canal. Stimuli were generated digitally (A0-6; National Instruments, Austin, TX). The tone pip frequencies for the second primary, f_2, were chosen to be 5.65, 8.0, 11.3, 16.0, 22.65, 32.0, and 45.25 kHz. The first primary, f_1, was related to the second primary by the equation: $f_2 = 1.2f_1$. The amplitude of the f_1 tone was initially small enough to not produce a detectable response; the amplitude was then increased by 5 dB sound pressure level (SPL) increments up to 80 dB SPL. The f_2 sound pressure level was always 10 dB less than the f_1 sound pressure level. The sound pressure emitted out of the ear canal was amplified and digitally sampled at 20 μsec intervals (A-2000; National Instruments). Fast Fourier transforms were computed and averaged over five consecutive waveform traces. $2f_1$-f_2 DPOAE amplitude and the surrounding noise floor were extracted. DPOAE threshold was defined qualitatively as the lowest f_2 level above which the DPOAE amplitude was greater than the surrounding noise floor for all five traces.

Auditory Brainstem Response (ABR)

ABRs were recorded by inserting electrodes into the vertex, pinnae and tail of the mouse. ABR potentials were evoked with 5 msec tone pips at the same frequencies used for the DPOAE second primary tone f_2. The tone volume was raised by 5 dB increments from 10 dB below threshold up to 80 dB SPL. At each sound pressure level, 1,024 responses were amplified (80 dB), filtered (0.1-2 kHz), and averaged (with stimulus polarity alternated) using a LabVIEW data-acquisition system (National Instruments, Austin, TX). Waveforms were discarded when peak-to-peak amplitude exceeded 15 μV. ABR threshold was defined qualitatively as the lowest SPL at which a repeatable waveform could be measured.

3.3.2 Results

ABRs and DPOAEs thresholds were significantly elevated in the *Tectb* mutant mice compared to thresholds measured in wild types (experiments were conducted with Stephane Maison). These results are consistent with previous measurements (Russell et al., 2007). Figure 3-5 shows auditory brainstem response (ABRs) results from wild types and $Tectb^{-/-}$ mutant mice. Mutants demonstrated significant low frequency hearing loss below ~20 kHz (Figure 3-5). Thresholds were about 50-60 dB SPL higher for $Tectb^{-/-}$ over this range of frequencies. Similarly, distortion production otoacoustic emission measurements also revealed a reduction in sensitivity at low frequencies in mutants (Figure 3-6). These measurements collectively demonstrate that cochlear sensitivity in $Tectb^{-/-}$ mutant mice at low frequencies (< 20 kHz) is significantly reduced compared wild types.

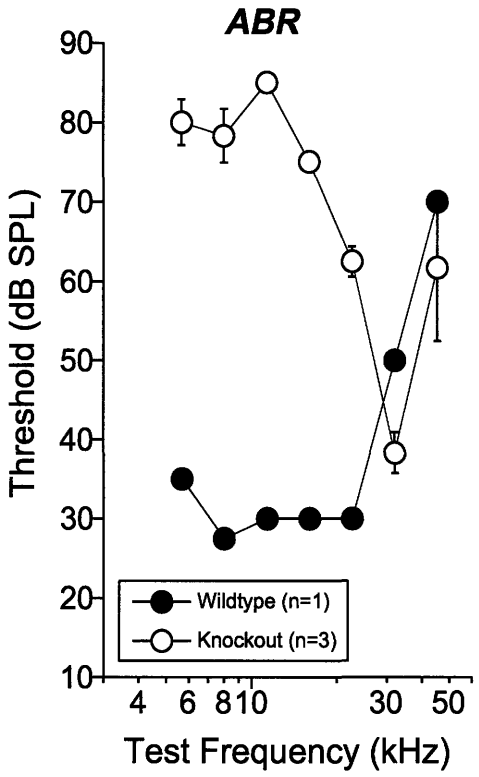

Figure 3-5: $Tectb^{-/-}$ mutant mice exhibited 50-60 dB SPL elevated thresholds at frequencies below 20 kHz. At high frequencies, the difference in sensitivity between mutants and wild types was smaller.

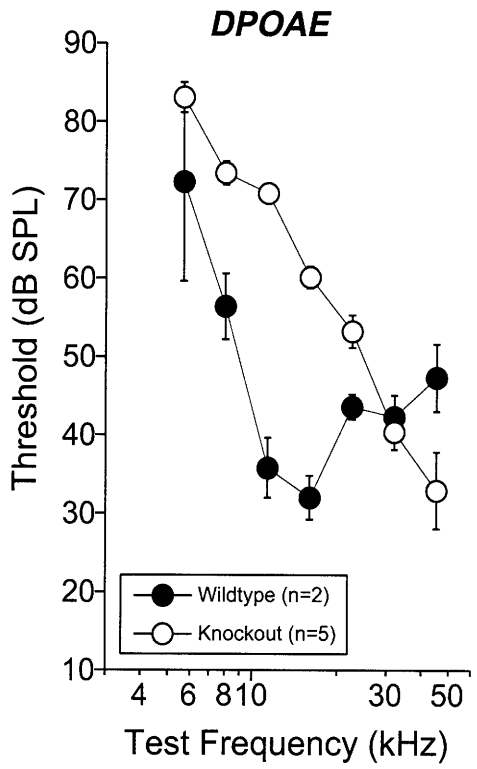

Figure 3-6: $Tectb^{-/-}$ mutant mice exhibited 20-35 dB SPL higher thresholds at frequencies between 10-20 kHz. At high frequencies, the difference in sensitivity between wild types and mutants was small (~10 dB SPL).

Chapter 4

The Role of Fixed Charge in the Mammalian Tectorial Membrane

Abstract

The tectorial membrane (TM) clearly plays a mechanical role in the cochlea. The presence of charged macromolecules in the TM suggests that electrical properties may contribute to this mechanical role. To investigate the role of fixed charge, we developed a microfabricated planar patch clamp technique to quantify the fixed charge density (c_f) of the TM. The TM was placed as an electrochemical barrier between two baths of differing ionic strength. Fixed charges in the TM created a Donnan potential difference between the baths. This potential depends on the fixed charge density, c_f, of the TM and on the ionic strength of the baths. Thus by measuring the potential difference at several ionic strengths, we can determine the c_f of the TM. We tested the validity of this technique on samples of poly(methacrylic acid) (PMAA) hydrogels with known charge density. We then applied the planar patch clamp technique to measure the c_f of TM samples. In both hydrogels and TM segments, electrical recordings were stable and repeatable. Furthermore, in both systems, the dependence of potential on bath ionic strength was well fit by Donnan theory. TM segments excised from the apical and middle cochlear turns were found to contain -7.1 ± 2.0 mmol/L of fixed charge. Analysis of the mechanical effect of fixed charge suggests that electro-

static forces due to fixed charge can contribute to the compressive rigidity of the TM. To test the electro-mechanical effect of fixed charge in the TM, sinusoidal electric fields were applied to TM samples in a microchannel. These fields exerted force on the fixed charge and generated nanometer-scale displacements at audio frequencies (10-100 Hz). We estimate that 7.1 mmol/L of fixed charge can contribute 0.35 kPa to the equilibrium bulk modulus of the TM and can drive electrical-to-mechanical transduction.

Key words: Hearing, cochlea, tectorial membrane, fixed charge, gel model, bulk modulus.

4.1 Introduction

Mechanical stimulation of mechano-sensory receptors in the mammalian cochlea is a pivotal event that underpins our remarkable sense of hearing (Hudspeth, 1985). The sensory receptors are functionally divided into two types: the inner and outer hair cells (OHCs). Both types of hair cells consist of stereociliary hair bundles, which project from the apical surface of the cells toward the undersurface of a gelatinous matrix called the tectorial membrane (TM). The OHC hair bundles are embedded in the TM and the inner hair cell (IHC) bundles are coupled to the TM through fluid in the sub-tectorial space. Based on the strategic location of the TM relative to the hair bundles, it is widely believed that the TM mechanically stimulates the hair bundles. However, the molecular origin of TM mechanical properties remains unclear (Freeman, Masaki, McAllister, Wei and Weiss, 2003).

Biochemical studies have long established that, in addition to collagen and glycoproteins, the TM contains highly charged glycosaminoglycans (GAGs) (Steel, 1983a; Steel, 1983b; Richardson et al., 1987; Thalmann et al., 1987; Suzuki et al., 1992; Thalmann et al., 1993; Killick et al., 1995). In similar charged connective tissues, electrostatic repulsion effects attributed to fixed charge contribute significantly to compressive stiffness. In cartilage, approximately 50% of the equilibrium modulus arises from

the presence of fixed charge (Buschmann and Grodzinsky, 1995). Because the TM has similar fixed charge constituents to cartilage, quantifying the density of charge in the TM is important for understanding the mechanical properties of the TM. Traditional electrical recording techniques that require micropipets have been largely unsuccessful in measuring TM fixed charge density because producing stable voltages across the TM have proven difficult (Steel, 1983a). Such measurements are complicated by the fact that the TM lacks an insulating cell membrane layer, thus making it difficult for the tip of a microelectrode to be topologically inside the TM. Here we present a novel technique to measure the fixed charge density (c_f) of the TM. We show that fixed charge is responsible for the compressive rigidity of the TM based on a macrocontinuum model and demonstrate that the TM exhibits electrically-evoked displacements at audio frequencies. This type of electrical-to-mechanical transduction is consistent with electrokinetic phenomena (Frank and Grodzinksy, 1987a; Frank and Grodzinksy, 1987b; Frank et al., 1990) and raises the intriguing notion that the TM may exert force on the hair bundles in the presence of electric fields generated by hair cell transduction currents (Hudspeth, 1982; Howard and Hudspeth, 1988; Pickles and Corey, 1992; Kennedy et al., 2005; Chan and Hudspeth, 2005a).

4.2 Materials and Methods

4.2.1 PMAA Gel Preparation

To test the validity of the planar patch clamp technique, we measured the c_f of polymethacrylic acid (PMAA) hydrogels. The chemical composition of PMAA gels has been previously described (Quinn and Grodzinsky, 1993). To match the size of the TM, PMAA gel solutions were injected between two glass slides. A coverslip (~200-300 μm in thickness) was used as a spacer between the slides. PMAA gel solution was injected between these glass slides. The slides containing the PMAA solution were then placed in 60° C water for 4 h to allow the gel to polymerize. Upon polymerization, the hydrogels were removed from the slides using a sharp razor blade.

They were washed in deionized water and then placed in an unbuffered 50 mM KCl solution at pH 11 for two days. The gel samples were then placed in a 50 mM KCl bath at physiological pH for an additional two days (Quinn and Grodzinsky, 1993).

4.2.2 Isolated TM Preparation

TM segments ($n = 5$ TM preparations) were excised from the cochleae of adult male mice (strain CD-1, 4-10 weeks old, Taconic) using a previously published surgical technique (Shah et al., 1995). The cochlea was surgically removed and placed in an artificial endolymph bath containing 174 mM KCl, 5 mM Hepes, 3 mM dextrose, 2 mM NaCl, and 0.02 mM $CaCl_2$. The bath was equilibrated at pH 7.3 at room temperature. The bone casing of the cochlea was gently chipped away until the organ of Corti was exposed. A combination of bright and dark-field illumination with a dissection microscope (Zeiss) provided visual access to the TM above the organ of Corti. A sterilized eyelash was used to remove Reissner's membrane and to lift the TM from the cochlea. TM segments (typically 0.5-1 mm in length) were isolated from the organ and placed in a fresh artificial endolymph bath. The care and use of animals in this study (NIH Grant R01 DC00238) were approved by the Massachusetts Institute of Technology Committee on Animal Care.

4.2.3 Measuring c_f with a Microfabricated Planar Patch Clamp

Isolated TM segments were mounted in a two-compartment chamber containing a glass-drilled microaperture (15 μm radius) (Lenox Laser, MD) connecting the two compartments. The underlying microchannel was cast in a transparent polymer called (poly)dimethylsiloxane (PDMS) by applying a standard soft lithography technique (McDonald et al., 2000; Whitesides et al., 2001). Briefly, PDMS replica of the underlying channel was cured and subsequently sealed to a glass slide containing the microaperture*. The TM was positioned to cover the microaperture so that an

*A detailed description of chamber and methods is included in the Appendix section of this chapter.

electro-chemical barrier separating the solutions in the two compartments was formed (Figure 4-1). The DC voltage difference (V_D) between the two compartments was measured with Ag/AgCl microelectrodes (A-M Systems, WA) containing 3 M KCl solution in agar. The electrodes were coupled to an amplifier (DAM60-G Differential Amplifier, World Precision Instruments, FL) that drove a multimeter (TX3 True RMS Multimeter, Tektronix). The top bath was perfused with artificial endolymph and the fluid channel was perfused with artificial endolymph-like solutions in which only the KCl concentration was varied. KCl concentrations of 21 mM, 32 mM, 43 mM, 87 mM, and 174 mM were used. Voltages were recorded in 2-3 second intervals for each test solution. Each test bath was perfused twice to test for repeatability.

The electric potential difference between the two baths depends on the ionic concentration of the two baths and on the fixed charge density of the TM in this configuration. Therefore, by measuring the electric potential difference across the TM, we can estimate TM fixed charge density (see Materials and Methods). The potential difference arises primarily from Donnan potentials that form between each bath and the TM, due to the presence of fixed charge. The potential between each bath and the TM is

$$V = \frac{RT}{F} \ln\left(\sqrt{\left(\frac{c_f}{2C_\Sigma}\right)^2 + 1} + \frac{c_f}{2C_\Sigma}\right), \tag{4.1}$$

where V is the potential of the TM relative to the bath, R is the molar gas constant, T is absolute temperature, F is Faraday's constant, c_f is the concentration of fixed charge within the TM, which can be either a positive or negative quantity, and $C_\Sigma = (1/2)\Sigma_i c_i$ is one half the sum of the concentrations c_i of each ion in the bath. Since the bath consisted mainly of KCl, we estimated $C_\Sigma = (1/2)(c_K + c_{Cl})$. If the two baths have identical compositions, the Donnan potential between the TM and each bath is identical, so the net potential difference between baths is zero. If one bath has a lower ionic concentration, the magnitude of the Donnan potential increases, so the potential difference between baths deviates from zero in a manner that depends on c_f within the TM. When the two baths have dissimilar ionic strengths, in addition to the Donnan potential, a liquid junction potential (LJP) can arise between the

baths. To accurately measure the Donnan potential, it is important to minimize and measure the LJP. In this respect it is convenient that the TM normally resides in endolymph, which consists primarily of K^+ and Cl^-. Since these two ions have similar mobilities, the junction potential resulting from a concentration difference between baths is minimized.

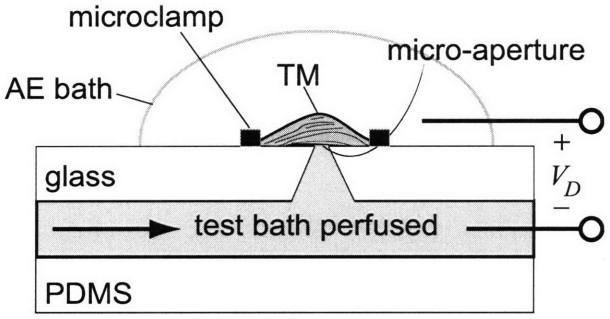

Figure 4-1: Microfabricated planar patch clamp chamber. Isolated TM segment in the chamber acts as an electrochemical barrier between the top bath and underlying test bath. The microaperture is a circular opening drilled through glass with a 15 μm radius on its surface that contacts the TM. The baths were continuously perfused to introduce different ionic strength solutions in the fluid channel and to ensure that the TM was immersed in fresh solution. The TM was kept stationary and stable over the microaperture with a microfabricated clamp. The potential difference between the baths (V_D) was recorded with Ag/AgCl electrodes that were placed in contact with the two baths.

4.2.4 Applying Electric Fields with a Microchannel Chamber

The microchannel chamber (Figure 4-2) was a 16 mm long channel cast in PDMS (McDonald et al., 2000; Whitesides et al., 2001). The cross-sectional area of the channel (1500×250 μm^2) was strategically designed to be large compared to the radial width and thick-

ness of the TM ($\sim$200$\times$40 μm^2). Holes were punched in the PDMS to allow two Ag/AgCl electrodes to access the fluid in the channel. The electrodes were placed $\sim$15 mm apart from each other. To create a seal for fluid perfusion, the channel was clamped to a glass slide.

Prior to clamping, the surface of the glass slide was coated with Cell-Tak (BD Biosciences, MA). This coating promoted adhesion of the TM to the glass surface. The TM was placed at the midpoint between the electrodes with its radial fibers oriented parallel to the direction of the applied electric field. Electrically-evoked displacements were measured with an optical imaging system.

In an additional series of experiments, we measured electrically-evoked displacements of the TM at different bath pHs. The artificial endolymph solution in the microchannel was initially equilibrated at pH 7.3. Acidic endolymph solution (pH 3.25) was then perfused through the microchannel until the pH of the bath became stable at pH 3.25. Displacements of the TM were measured at pH 7.3 and 3.25 in response voltage stimulus.

Motion Analysis with Optical System

The motion of the TM was measured optically with a 40$\times$ objective (Zeiss) and a transmitted light condenser (0.8 N.A.). Images were collected with a 12 bit, 1024 $\times$ 1024 pixel CCD camera (CAD7-1024A; Dalsa Inc., Waterloo, ON, Canada) by strobing the light-emitting diode (LED). The TM segment was illuminated at 16 evenly spaced stimulus phases over several stimulus cycles. The collected images were analyzed to determine the first 8 harmonics of the periodic motion. We computed the magnitude and phase of radial displacement from the series of collected images by using previously published motion tracking algorithms (Davis and Freeman, 1998; Aranyosi and Freeman, 2004).

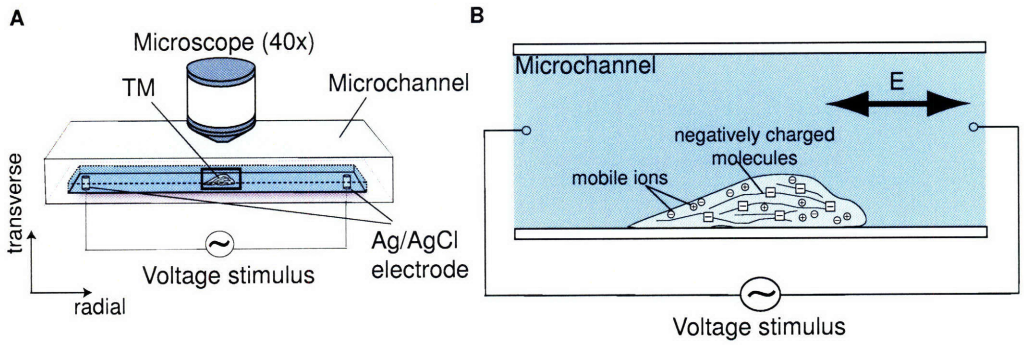

Figure 4-2: TM segments were positioned between a pair of Ag/AgCl electrodes. Voltage stimulus was applied through the electrodes and TM radial displacement was measured with an optical imaging system.

4.3 Results and Discussion

4.3.1 Fixed Charge Density of PMAA Gels

To test the validity of the planar patch clamp technique, we first measured the c_f of polymethacrylic acid hydrogels (Figure 4-3). Voltage measurements were conducted over the course of approximately 50 minutes and were found to be stable and repeatable. A Donnan fit to the voltage recordings versus test bath ionic concentrations yielded a c_f of -80 mmol/L (Figure 4-3B). This value is comparable to c_f estimates ($-$100-120 mmol/L) based on a separate titration experiment conducted by Quinn and Grodzinsky (Quinn and Grodzinsky, 1993).

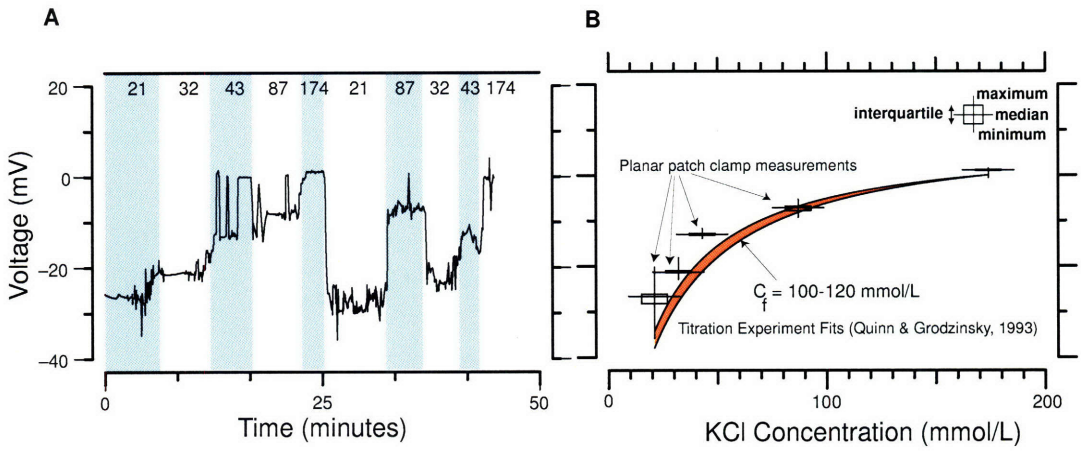

Figure 4-3: PMAA gels were positioned in microfabricated planar patch clamp chamber. (A) Voltages were stable and repeatable over several minutes up to an hour while different test baths were being perfused. The alternating shaded and white regions indicate times with different perfusates (21, 32, 43, 87, 174 mmol KCl). (B) PMAA gel voltages vs. test KCl concentration. Lines and orange region denote range of fits to the Donnan relation based on estimates of c_f (−100-120 mmol/L) from a titration experiment conducted by Quinn and Grodzinsky (Quinn and Grodzinsky, 1993). The value of c_f predicted from the best fit to the median values of the voltage data in the planar patch clamp experiment (−80 mmol/L) was comparable to the titration experiment.

4.3.2 Fixed Charge Density of the TM

Figure 4-4A shows typical voltage recordings over the course of approximately one hour for a TM sample. Measurements were repeated for each test bath solution to ensure that the measured voltages (V_D) were reproducible. The sharp transients to zero volts in Figure 4-4A were instances when the TM sample was intentionally removed from the aperture. This removal created an electrical short path between the two baths. TM voltages were fit by the Donnan relation. Based on the Donnan relation fit, the value of c_f was approximately -7.1 ± 2.0 mmol/L ($n = 5$ TM samples).

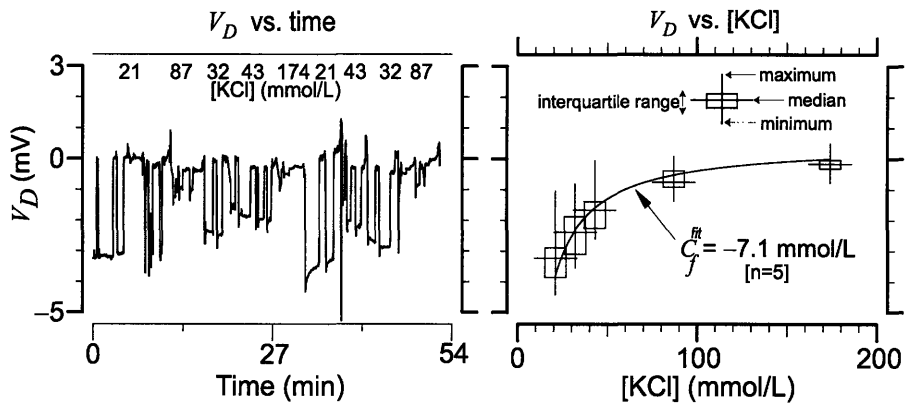

Figure 4-4: TM samples positioned in planar patch clamp chamber. (A) Voltages were stable and repeatable over several minutes up to an hour while different test bath solution were being perfused. The alternating shaded and white regions indicate times with different perfusates (21, 32, 43, 87, 174 mmol KCl). The sharp transients to zero volts resulted from intentionally shorting the two baths by lifting the TM from the aperture to check for drift in the measurement system. (B) Voltage was plotted as a function of test bath KCl concentration. The best fit to the median voltage values yielded c_f values of -7.1 ± 2.0 mmol/L ($n = 5$ TM preparations). Interquartile ranges are represented with vertical lines. The range denotes fits to the maximum and minimum values in the interquartile ranges.

4.3.3 Electrically-Evoked Displacements of the TM

Electric fields with amplitudes of 5 kV/m at 1 Hz in the microchannel induced periodic radial displacements of the TM with peak amplitudes up to 850 nm (Figure 4-5A). The polarity of the voltage driven motions were consistent with the presence of negative fixed charge in the TM. To explore the mechanism responsible for this motion, we examined displacement amplitudes and phase at multiple frequencies. Displacement amplitudes decreased from 850 nm at 1 Hz to around 20 nm at 80 Hz. The phase lag (with respect to the input electrical stimulus) was around –55 to –90 degrees for 1–80 Hz (Figure 4-5B). Voltage-induced displacement scaled linearly with electric field

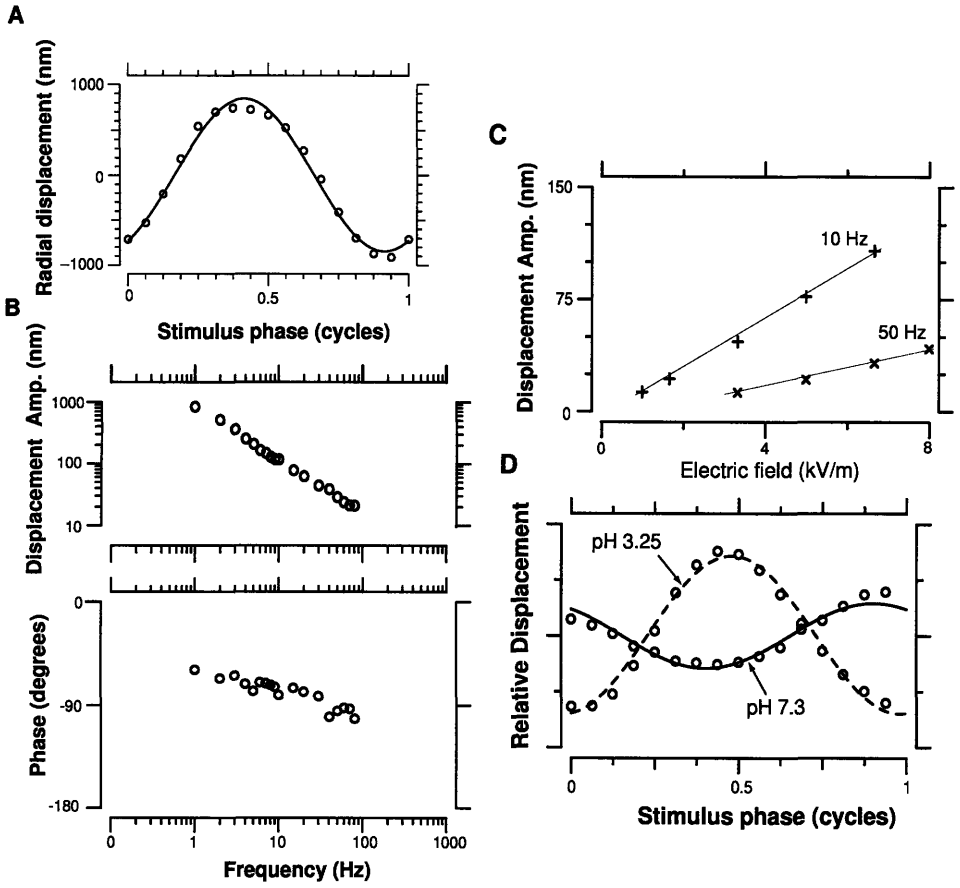

Figure 4-5: (A) Radial displacement at a location on the surface of the TM (in the region that normally overlies the OHC hair bundles) in response to a 1 Hz, 5 kV/m stimulus. Symbols denote measured points; the line connecting these points is the sum of the harmonic components for the measurements. Displacement amplitude was ~850 nm and lagged the stimulus in phase by around -55 degrees. (B) Magnitude and phase of TM motion as a function of frequency (1-80 Hz) in response to 5 kV/m. TM displacement decreased with frequency. The phase was between -55 degrees and -90 degrees over this range of frequencies. (C) TM displacement amplitude vs. electric field magnitude at 10 Hz and 50 Hz. Solid lines denote linear regressions through the origin with coefficient of correlation $R = 0.998$ for 10 Hz and $R = 0.99$ for 50 Hz. (D) Voltage-induced radial displacement of a TM sample vs. stimulus phase at two different bath pHs (pHs 7.3 and ~3.25).

amplitude as shown for 10 Hz and 50 Hz in Figure 4-5C.

Figure 4-5D shows a phase shift in the TM's voltage-induced displacements that occurred after equilibration at pH 3.25. The motion underwent a phase transition close π radians indicating that the sign of the fixed charge in the TM may have changed.

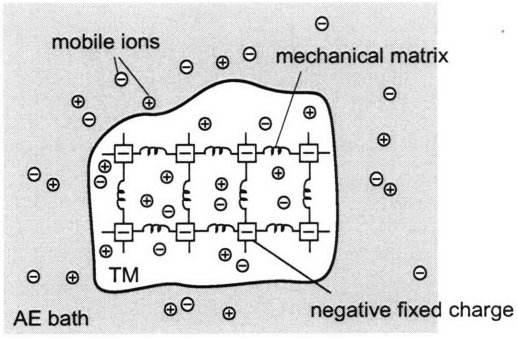

Figure 4-6: Electrostatic repulsion effects driven by fixed charge contribute to the equilibrium bulk modulus of the TM. This mechanical effect of fixed charge is significant even in the presence of shielding by mobile counterions. Approximately 70% of the equilibrium bulk modulus of the TM is due to the presence of fixed charge.

4.3.4 Fixed Charge Contributes to Compressive Stiffness of the TM

Fixed charge can contribute to the mechanical properties of connective tissues through electrostatic forces (Buschmann and Grodzinsky, 1995). To test this concept, we applied a macrocontinuum model based on Donnan equilibrium (Figure 4-6) to predict the bulk modulus (κ) of the TM resulting solely from -7.1 mmol/L of fixed charge. We assumed that fixed charge groups were isotropically distributed, the electric potential was spatially invariant, and mobile ions were in the fluid phase of the TM. The characteristic dimensions in this macrocontinuum model are large compared to the electrical Debye length so that electroneutrality is also assumed valid within the TM. This model predicts that electrostatic repulsion effects of fixed charge can contribute up to 0.35 kPa to the equilibrium bulk modulus of the TM. This accounts for approx-

imately 70% of compressive rigidity of the TM at equilibrium (Masaki et al., 2006).

4.3.5 Electrical-to-Mechanical Transduction Mechanism

In connective tissues, like cartilage, electric fields have been demonstrated to exert forces on the fluid phase of the tissue, which in turn causes an electro-osmotic convection of fluid (Frank and Grodzinksy, 1987a). Electric fields can concurrently drive the motion of the solid matrix through electrophoresis. The electrically-evoked displacements of the TM (Figure 4-5A) were indicative of an electrophoretic mechanism. TM displacements were largest at lowest frequencies, consistent with electrokinetic transduction theory. Figure 4-5B shows that electrically-evoked displacements decreased with frequency. This decrease is likely due to the fact that it takes a finite time for electro-osmotic flow of the fluid phase and electrophoretic motion of the solid phase to occur in response to high frequency electrical stimulation (Frank and Grodzinksy, 1987a). In Figure 4-5C, TM displacement increased linearly with electric field magnitude, which is also consistent with electrokinetic theory (Frank and Grodzinksy, 1987a). In electrokinetic transduction, a current-generated stress response was predicted to be linearly proportional to the amplitude of an applied current density (Frank and Grodzinksy, 1987a; Frank and Grodzinksy, 1987b).

To understand why TM displacement changed phase by $\sim\pi$ radians at pH 3.25 relative to pH 7.3 requires an understanding of the effect bath pH can have on fixed charge. Changing the pH of a bath can alter the ionization state of fixed charge groups (Weiss and Freeman, 1997b). Since about 50% of the TM's dry weight consists of GAGs and collagen (Richardson et al., 1987), the effect of pH on the TM can be explained in the way these constituents ionize as a function of pH. The GAGs in the TM carry sulfate (SO_3^-) and carboxyl (COO^-) charge groups. The charges on both of these charge groups are fully ionized at physiological pH and are neutralized at acidic pH values (pKs between 2-4). In contrast, collagen contains amino groups (NH_3^+) along with carboxyl groups. At physiological pH, the net charge on collagen is small because the net charge of amino and carboxyl groups is zero. But at acidic pH, the carboxyl groups are neutralized leaving the amino groups, which still carry

a net positive charge. Therefore, the net fixed charge of the TM is positive at acidic pH because of the ionized amino groups of collagen (Weiss and Freeman, 1997b; Weiss and Freeman, 1997a). This sign reversal in the net fixed charge of the TM is consistent with TM displacement undergoing close to a π radians phase shift at pH 3.25 compared to pH 7.3 (Figure 4-5D).

4.3.6 Implications for Previous Electrical Studies of the Cochlea

Electrically-evoked displacements of the TM have important implications for studies that have used electrical stimulation to drive the cochlear partition (Reuter et al., 1992; Xue et al., 1995; Scherer and Gummer, 2005; Chan and Hudspeth, 2005a; Nowotny and Gummer, 2006; Karavitaki and Mountain, 2007). In a number of *in situ* studies, electrical stimulation has been used to drive the cochlear partition (organ of Corti and the TM). Electrodes were typically placed directly above and below the cochlear partition and current was passed between the electrodes to stimulate the electromotile response of OHCs. The observed motions of the partition in these studies were attributed entirely to OHC electromotility. However, the fact that the TM is electrokinetic indicates that the TM may also exhibit motion in response to electrical stimulation. Although nanometer scale displacements of the TM were induced only in response to rather large electric fields (> 1 kV/m), it is important to note that the TM was bound to a glass slide in our measurements. This boundary constraint likely dampened TM displacement, suggesting that displacements of the TM are likely to be substantially larger *in situ*. Therefore, electrically-evoked displacements of the TM may affect the interpretation of OHC motility in studies that electrically stimulate the entire cochlear partition.

4.3.7 Implications for Cochlear Mechanics

The fact that the TM is located in close proximity to the tips of the hair bundles suggests that physiological electrical currents may exert force on the TM. While it is difficult to determine the strength of the electric fields generated by hair cell

mechano-transduction, the insertion of the OHC hair bundles into the undersurface of the TM suggests that local electric fields around the hair bundles (Hudspeth, 1982) may be strong enough to generate local displacements on the surface of the TM. Hudspeth (1982) estimated that the electric fields within 1 μm of the hair bundle tips were $\sim$ 1-5 V/m in the saccular macculae of the bull frog. These electric fields are significantly smaller than the electric fields applied in the microchannel chamber by up to three orders of magnitude. However, the TM was constrained on an entire surface in the microchannel, suggesting that electrically-evoked displacements of the TM may be significantly larger *invivo*, since the TM is largely unconstrained above the hair bundles. Therefore, electrically-evoked displacements of the TM may generate enough force to deflect the hair bundles and to participate in cochlear amplification.

4.4 Appendix

This section provides supplementary methods and results that were not included in the earlier sections. In the methods section, I describe how soft lithography techniques were used to microfabricate the planar patch clamp chamber and the microchannel. The methodologies described here have been previously reported by others (McDonald et al., 2000; Whitesides et al., 2001). I will also present a novel way of applying electric fields to the TM in the transverse direction with the planar patch clamp setup. Instead of recording voltages while the TM was placed over the microaperture, electric fields were applied to the TM.

The results section presents electrically-evoked displacement measurements of the TM in the microaperture configuration.

4.4.1 Additional Methods

Microfluidic Systems

Microfluidic devices are currently being applied across several industries ranging from medical devices to environmental monitoring and biochemical analysis (McDonald

and Whitesides, 2002). One of the current methodologies applied to engineer these kinds of devices is a low-cost, fast solution to microfabrication called soft lithography. Soft lithography exploits the optical and chemical properties of PDMS. The design of the microchannel and the planar patch clamp chambers applied PDMS to replicate the micron-scaled features of a microchannel pattern molded on silicon wafers (McDonald et al., 2000; Whitesides et al., 2001; McDonald and Whitesides, 2002).

PDMS is usually packaged as two separate fluid parts: a base and a curing agent. Mixing the base and the curing agent (10:1 base volume to curing agent volume ratio) causes vinyl groups in the base to react with silicon hydride groups in the curing agent, which forms an elastomeric solid over the course of several hours at room temperature. Pouring this mixture over a mold that contains nanometer-scale features allows the mixture to take the form of the mold and to harden in the shape of the mold. This technique allows the replication of complex patterns.

Soft Lithography Technique

The pattern of the microchannels was first designed in a CAD program and printed on a high resolution printer at Pageworks Inc. (Cambridge, MA.). The transparencies were used as a photomask to create the patterns on the master by photolithography (McDonald and Whitesides, 2002). Figure 4-7 shows the typical steps taken to create a PDMS replica of a microchannel. The end result is a solid PDMS replica that was sealed to a glass slide. The microchannel and planar patch clamp chambers were microfabricated using this type of process.

Microaperture Chamber

The microaperture setup was identical to the planar patch clamp chamber. But instead of recording voltages, the microaperture configuration was used to apply voltages to the TM.

Isolated segments of the TM were immersed artificial endolymph and placed over a 12.5 μm radius aperture (Lenox Laser, MD) that separated two fluid compartments. Sinusoidal voltages applied between the compartments generated electric fields in the

region of the TM covering the aperture (Figure 4-8). Displacements were visualized in the transverse direction at multiple focal planes within the bulk of the TM (Figure 4-9).

4.4.2 Additional Results

Electrically-Evoked Displacements of the TM in the Transverse Direction

Electrically-evoked transverse displacements of the TM in the microaperture chamber were measured across multiple frequencies and electric field amplitudes. Figure 4-10A shows that transverse displacements had a peak amplitude of 50 nm in response to 8 kV/m at 10 Hz. Displacements decreased as a function of stimulus frequency (Figure 4-10B) and increased with electric field level (Figure 4-10C), consistent with electrokinetic theory (Frank and Grodzinksy, 1987a).

For a given electric field stimulus, transverse displacements of the TM were some what smaller than radial displacements of the TM measured in the microchannel (Figure 4-5). This difference may be caused by the different boundary conditions in the two experimental setups. In the microaperture setup, the electric fields were largest only in the region directly above the microaperture (12.5 μm radius). In contrast, TM segments in the microchannel were stimulated by electric fields that exerted large radial forces over the entire structure of the TM.

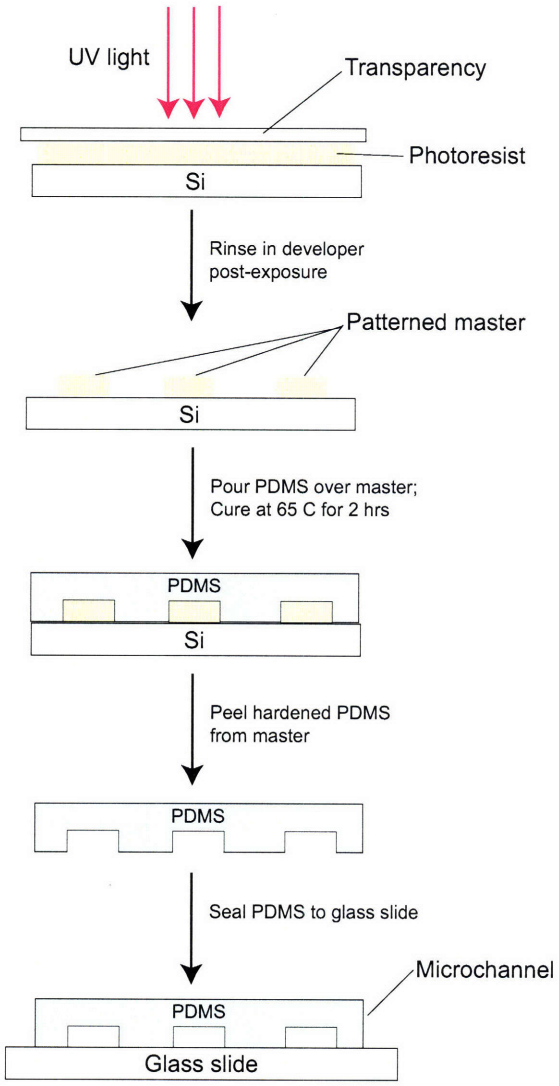

Figure 4-7: Channel patterns were initially designed in a CAD program and printed as a transparency using a high resolution printer. The transparency was placed over a silicon wafer (master) containing a spin-coated layer of photoresist (~200-300 μm thick). The apparatus was exposed to ultra-violet (UV) radiation. The areas of the photomask that were transparent allowed exposure of the photoresist to the UV rays. These regions served as permanent molds on the master. Pouring PDMS over the wafer allowed the PDMS to morph to the shape and size of the molds. Heating at 65° C allowed the PDMS to harden over the master. The hardened PDMS was then pealed from the master and sealed to a glass slide to create an enclosure for the channel (Adapted from McDonald and Whitesides, 2002).

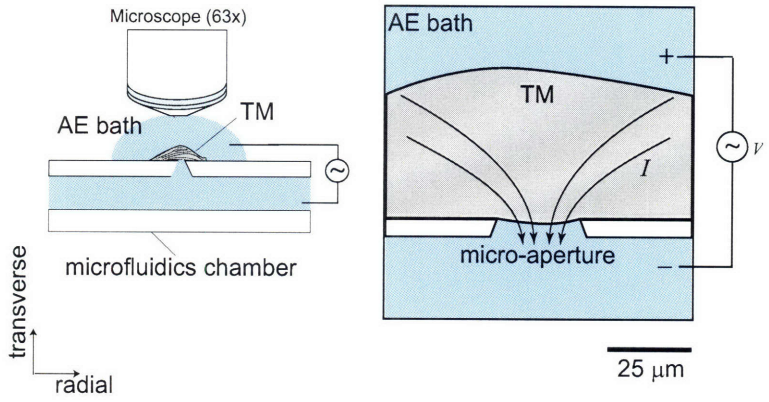

Figure 4-8: (A) The TM was placed over an aperture separating two baths. Electrically-evoked displacements of the TM were measured with an optical system (63× objective) in the transverse direction. (B) Voltages were delivered with Ag/AgCl electrodes that were placed in contact with the top bath and the underlying fluid channel. Electric field strength was greatest in the region directly above the microaperture.

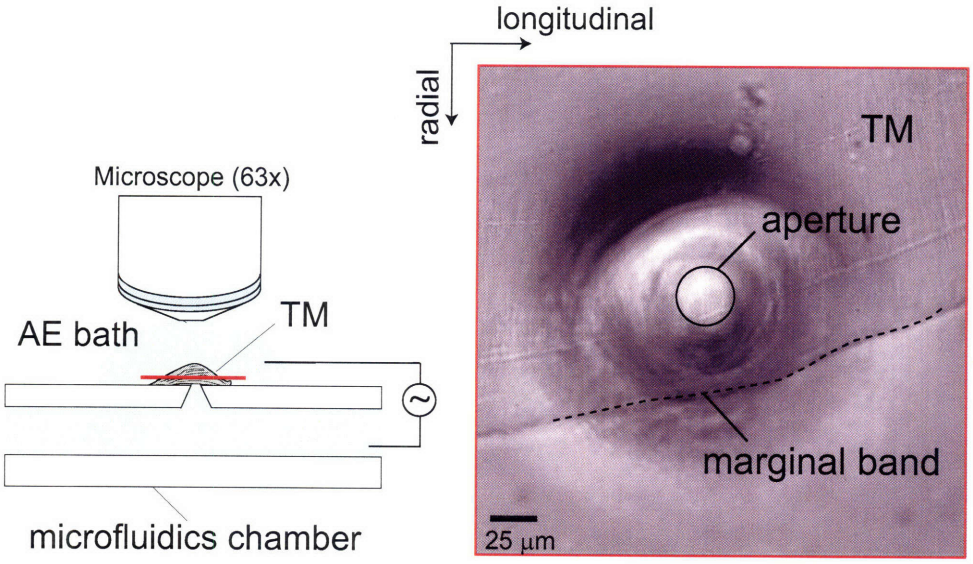

Figure 4-9: Left: TM segment was imaged at multiple focal planes separated by 1 μm step sizes. Red line denotes a focal plane above the surface of the glass. Right: Light microscope image taken of the TM over the microaperture. Dotted line denotes the marginal band boundary. Transverse displacements of the TM were measured directly over the microaperture. TM displacements were largest in this area where the electric field was largest.

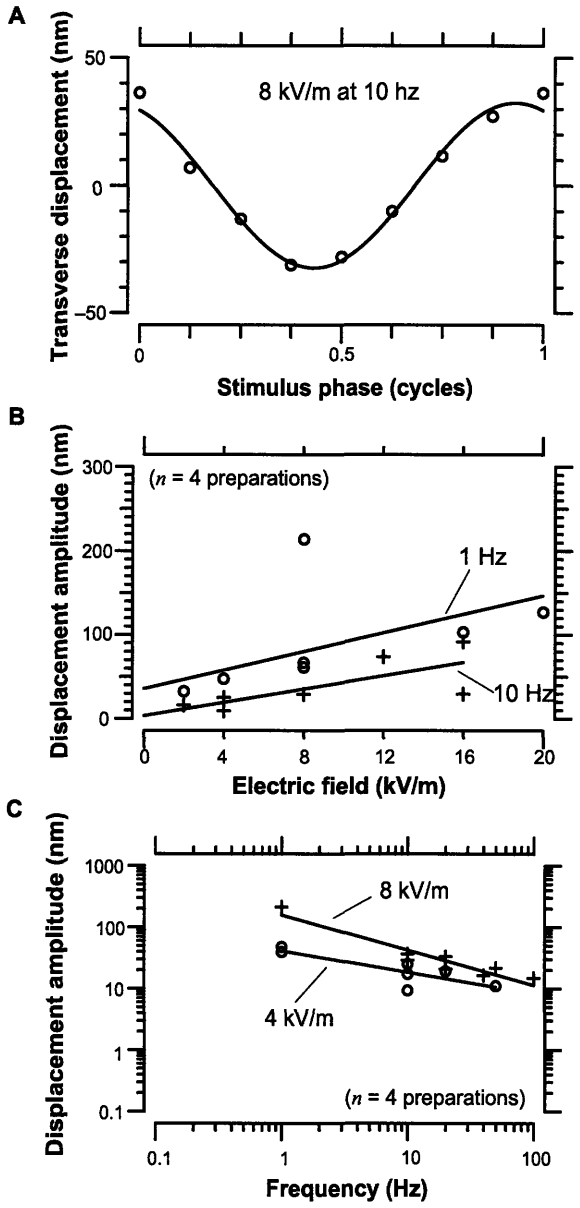

Figure 4-10: (A) The TM exhibited nanometer-scale transverse displacements at audio frequencies. (B) Displacements scaled linearly with electric field amplitude. (C) Transverse displacement decreased with increasing stimulus frequency over the range of frequencies tested (1-50 Hz).

Chapter 5

Conclusions

The following is a comprehensive list of conclusions based on the findings presented in the preceding chapters of this thesis:

1) We have demonstrated that radial displacements of an isolated TM excite waves of motion that propagate longitudinally with velocities similar to those of the BM traveling wave. Analysis of physiological loading effects of the hair bundles, the limbal attachment of the TM, and fluid viscosity in the subtectorial space suggests that TM waves also can propagate *in vivo*.

2) Mutations targeting glyco-proteins in the TM (beta-tectorin) can cause changes in TM mechanical properties and alter TM waves. These changes in wave motion along *Tectb* mutant TMs were correlated with the loss of cochlear sensitivity and sharpened frequency tuning measured in $Tectb^{-/-}$ mutant mice (Chapter 3).

3) In Chapter 4, we showed that fixed charge can contribute to the compressive stiffness of the TM at equilibrium. Moreover, fixed charge also is responsible for electrically-evoked displacements of the TM. Electrical-to-mechanical transduction of the TM raises the intriguing notion that transduction currents in the cochlea may exert forces on the TM, which in turn can contribute to hair bundle deflection.

4) Although the analysis on the mechanical role of fixed charge is limited to compressive stiffness, it is likely that the shear storage modulus, G', and the shear viscosity, η, of the TM are also affected by the presence of fixed charge. The fact that the striated sheet matrix is missing in $Tectb^{-/-}$ mice suggests that the fixed charge

density, c_f, of the TM may be significantly changed in these mice. Therefore, the mechanical properties of the TM that are responsible for waves may originate in part from the mechanical effects of fixed charge.

5) The most significant conclusion from this thesis is the concept that the cochlea can support two traveling waves (Figure 5-1). The contribution of TM waves is expected to be significant only in the region where the TM and BM waves have comparable wavelengths and propagation velocities and are likely to be in phase with respect to each other. The spatial extent of this region is likely to correspond to frequencies within approximately half an octave to one octave of the characteristic frequency. The concept that the mammalian cochlea supports two traveling waves with similar propagation velocities over a limited spatial region has been suggested in a previous cochlear model (Hubbard, 1993), where the combination of the two traveling waves was shown to produce sharp tuning and emissions.

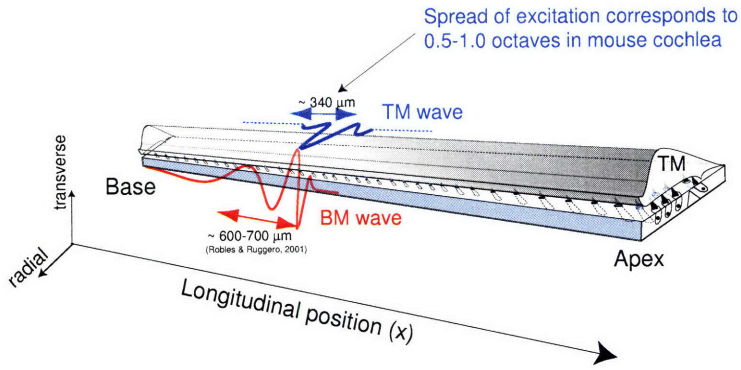

Figure 5-1: The TM (blue) and BM (red) waves may interact over a limited spatial region where the two waves have comparable wavelengths and velocities. Through feedback and coupling via the outer hair cells (OHCs), the radial motion of the TM wave can help drive OHC motility and amplify the transverse motion of the BM wave. Based on this kind of mechanism, the BM and TM waves may amplify each other's motion and thereby play a key role in the stimulation of hair cells and cochlear amplification.

Bibliography

Abnet, C. C. (1998). *Measuring the mechanical properties of the tectorial membrane with a magnetizable bead*, PhD thesis, Massachusetts Institute of Technology, Cambridge, MA.

Abnet, C. C. and Freeman, D. M. (2000). Deformations of the isolated mouse tectorial membrane produced by oscillatory forces, *Hear Res* **144**: 29–46.

Alberts, B., Bray, D., Lewis, J., Raff, M., Roberts, K. and Watson, J. D. (1994). *Molecular Biology of the Cell*, 3rd edn, Garland Publishing, New York.

Allen, J. B. (1980). Cochlear micromechanics — a physical model of transduction, *J Acoust Soc Am* **68**: 1660–1670.

Aranyosi, A. J. and Freeman, D. M. (2004). Sound-induced motions of individual cochlear hair bundles, *Biophys J* **87**: 3536–3546.

Billone, M. and Raynor, S. (1973). Transmission of radial shear forces to cochlear hair cells, *J Acoust Soc Am* **54**: 1143–1156.

Brownell, W. E., Bader, C. R., Bertrand, D. and de Ribaupierre, Y. (1985). Evoked mechanical responses of isolated cochlear hair cells, *Science* **227**: 194–196.

Buschmann, M. D. and Grodzinsky, A. J. (1995). A molecular model of proteoglycan-associated electrostatic forces in cartilage mechanics, *J Biomech Eng* **117**: 179–192.

Chan, D. K. and Hudspeth, A. J. (2005a). Ca^{2+} current-driven nonlinear amplification by the mammalian cochlea in vitro, *Nat Neurosci* **8**: 149–155.

Chan, D. K. and Hudspeth, A. J. (2005b). Mechanical responses of the organ of corti to acoustic and electrical stimulation in vitro, *Biophys J* **89**: 4382–4395.

Chen, S., Fatemi, M. and Greenleaf, J. F. (2004). Quantifying elasticity and viscosity from measurement of shear wave speed dispersion, *J Acoust Soc Am* **115**: 2781–2785.

Dallos, P. (1996). Overview: Cochlear neurobiology, *in* P. Dallos, A. N. Popper and R. R. Fay (eds), *The Cochlea*, Vol. 8 of *Springer Handbook of Auditory Research*, Springer-Verlag, New York.

Davis, C. Q. and Freeman, D. M. (1998). Using a light microscope to measure motions with nanometer accuracy, *Opt Eng* pp. 1299–1304.

Davis, H. (1958). A mechano-electrical theory of cochlear action, *Ann Otol Rhinol Laryngol* **67**: 789–801.

de Boer, E. (1996). Mechanics of the cochlea: modeling efforts, *in* P. Dallos, A. N. Popper and R. R. Fay (eds), *The Cochlea*, Vol. 8 of *Springer Handbook of Auditory Research*, Springer-Verlag, New York.

de Boer, E. (1997). Classical and non-classical models of the cochlea, *J Acoust Soc Am* **101**: 2148–2150.

Eikenberry, E. F., Mendler, M., Burgin, R., Winterhalter, K. H. and Burckner, P. (1991). Fibrillar organization in cartilage, *Articular Cartilage and Osteoarthritis*, Raven Press, New York, pp. 133–149.

Eyre, D. R. and Wu, J. (1995). Collagen structure and cartilage matrix integrity, *J Rheumatol Suppl* **43**: 82–85.

Frank, E. and Grodzinksy, A. J. (1987a). Cartilage electromechanics: I. Electrokinetic transduction and the effects of electrolyte pH and ionic strength, *J Biomech* **20**: 615–627.

Frank, E. and Grodzinksy, A. J. (1987b). Cartilage electromechanics: II. A continuum model of cartilage electrokinetics and correlation with experiments, *J Biomech* **20**: 629–639.

Frank, E. H., Grodzinsky, A. J., Phillips, S. L. and Grimshaw, P. E. (1990). Physiochemical and bioelectrical determinants of cartilage material properties, *in* V. C. Mow, A. Ratcliffe and S. L. Y. Woo (eds), *Biomechanics of Diarthrodial Joints: Volume 1*, Springer-Verlag, New York, pp. 261–282.

Freeman, D., Abnet, C., Hemmert, W., Tsai, B. and Weiss, T. (2003). Dynamic material properties of the tectorial membrane: A summary, *Hear Res* **180**: 1–10.

Freeman, D. M. and Weiss, T. F. (1985). *in* J. B. Allen, J. L. Hall, A. Hubbard, S. T. Neely and A. Tubis (eds), *Peripheral Auditory Mechanisms*, Springer-Verlag, New York, pp. 147–154.

Freeman, D. M. and Weiss, T. F. (1990). Superposition of hydrodynamic forces on a hair bundle, *Hear Res* **48**: 1–16.

Freeman, D., Masaki, K., McAllister, A., Wei, J. and Weiss, T. (2003). Static material properties of the tectorial membrane: A summary, *Hear Res* **180**: 11–27.

Fridberger, A., Tomo, I., Ulfendahl, M. and de Monvel, J. B. (2006). Nanomechanics of the subtectorial space caused by electromechanics of cochlear outer hair cells, *Proc Natl Acad Sci USA* **103**: 1918–1923.

Ghaffari, R., Aranyosi, A. J. and Freeman, D. M. (2007). Longitudinally propagating traveling waves of the mammalian tectorial membrane, *Proc Natl Acad Sci USA* **104**: 16510–16515.

Goodyear, R. and Richardson, G. P. (2002). Extracellular matrices associated with the apical surfaces of sensory epithelia in the inner ear: Molecular and structural diversity, *J Neurobiol* **53**: 212–227.

Greenleaf, J. F., Fatemi, M. and Insana, M. (2003). Selected methods for imaging elastic properties of biological tissues, *Annu Rev Biomed Eng* **5**: 57–78.

Gu, J. W., Aranyosi, A. J., Hemmert, W. and Freeman, D. M. (2005). Measuring material properties of the tectorial membrane at audio frequencies with a microfabricated probe, *Abstracts of the Twenty-Eight Annual Midwinter Research Meeting*, Association for Research in Otolaryngology, New Orleans, Louisiana, p. 240.

Gueta, R., Barlam, D., Shneck, R. Z. and Rousso, I. (2006). Measurement of the mechanical properties of the tectorial membrane using atomic force microscopy, *Hear Res* **103**: 14790–14795.

Guinan, J., Lin, T. and Cheng, H. (2005). Medial-olivocochlear-efferent inhibition of the first peak of auditory-nerve responses: evidence for a new motion within the cochlea, *J Acoust Soc Am* **118**: 2421–2433.

Gummer, A. W., Hemmert, W. and Zenner, H.-P. (1996). Resonant tectorial membrane motion in the inner ear: its crucial role in frequency tuning, *Proc Natl Acad Sci USA* **93**: 8727–8732.

Hillery, C. M. and Narins, P. M. (1984). Neurophysiological evidence for a traveling wave in the amphibian inner ear, *Science* **225**: 1037–1039.

Horn, B. K. P. and Weldon Jr., E. J. (1988). Direct methods for recovering motion, *Internatl J of Computer Vision* **2**: 51–76.

Howard, J. and Hudspeth, A. J. (1988). Compliance of the hair bundle associated with gating of mechanoelectrical transduction channels in the bullfrog's saccular hair cell, *Neuron* **1**: 189–199.

Hubbard, A. (1993). A traveling-wave amplifier model of the cochlea, *Science* **259**: 68–71.

Hudspeth, A. J. (1982). Extracellular current flow and the site of transduction by vertebrate hair cells, *J Neurosci* **2**: 1–10.

Hudspeth, A. J. (1985). The cellular basis of hearing: the biophysics of hair cells, *Science* **230**: 745–752.

Jia, S. and He, D. Z. Z. (2005). Motility-associated hair-bundle motion in mammalian outer hair cells, *Nat Neurosci* **8**: 1028–1034.

Jia, S., Zuo, J., Dallos, P. and He, D. Z. Z. (2005). *in* A. L. Nuttall, T. Ren, P. Gillespie, K. Grosh and E. de Boer (eds), *Auditory Mechanisms*, World Scientific, Singapore, pp. 261–269.

Johnstone, J. R. and Johnstone, B. M. (1966). Origin of summating potential, *J. Acoust. Soc. Am.* **40**: 1405–1413.

Karavitaki, K. D. and Mountain, D. C. (2007). Evidence of outer hair cell driven oscillatory fluid flow in the tunnel of corti, *Biophys J* **92**: 3284–3293.

Keiler, S. and Richter, C. P. (2001). Cochlear dimensions obtained in hemicochleae of four different strains of mice: Cba/caj, 129/cd1, 129/svev and c57bl/6j, *Hear Res* **162**: 91–104.

Kennedy, H. J., Crawford, A. C. and Fettiplace, R. (2005). Force generation by mammalian hair bundles supports a role in cochlear amplification, *Nature* **24**: 880–3.

Kennedy, H. J., Evans, M. G., Crawford, A. C. and Fettiplace, R. (2006). Depolarization of cochlear outer hair cells evokes active hair bundle motion by two mechanisms, *Nat Neurosci* **8**: 2757–2766.

Killick, R., Legan, P. K., Malenczak, C. and Richardson, G. P. (1995). Molecular cloning of chick β-tectorin, an extracellular matrix molecule of the inner ear, *Journal of Cell Biology* **129**: 535–547.

Kössl, M. and Russell, I. J. (1995). Basilar membrane resonance in the cochlea of the mustached bat, *Proc Natl Acad Sci USA* **92**: 276–279.

Legan, P., Lukashkina, V., Goodyear, R., Kossl, M., Russell, I. and Richardson, G. (2000). A targeted deletion of α-tectorin reveals that the tectorial membrane is required for the gain and timing of cochlear feedback, *Neuron* **28**: 273–285.

Legan, P., Lukashkina, V., Goodyear, R., Lukashkin, A., Verhoeven, K., Camp, G., Russell, I. and Richardson, G. (2005). A deafness mutation isolates a second role for the tectorial membrane in hearing, *Nat Neurosci* **8**: 1035–1042.

Li, Y., Lacerda, D. A., Warman, M. L., Beier, D. R., Yoshioka, H., Ninomiya, Y., Oxford, J. T., Morris, N. P., Andrikopoulos, K., Ramirez, F., Wardell, B. B., Lifferth, G. D., Teuscher, C., Woodward, S. R., Taylor, B. A., Seegmiller, R. E. and Olson, B. R. (1995). A fibrillar collagen gene, col11a1, is essential for skeletal morphogenesis, *Cell* **80(3)**: 435–430.

Lim, D. J. (1972). Fine morphology of the tectorial membrane. its relationship to the organ of corti, *Arch Otolaryngol* **96**: 199–215.

Lim, D. J. (1980). Cochlear anatomy related to cochlear micromechanics. a review, *J Acoust Soc Am* **67**: 1686–1695.

Maison, S. F., Luebke, A. E., Liberman, M. C. and Zuo, J. (2002). Efferent protection from acoustic injury is mediated via α9 nicotinic acetylcholine receptors on outer hair cells, *J Neurosci* **22(24)**: 10838–10846.

Mammano, F. and Nobili, R. (1993). Biophysics of the cochlea: Linear appoximation, *J Acoust Soc Am* **93**: 3320–3332.

Masaki, K., Weiss, T. F. and Freeman, D. M. (2006). Poroelastic bulk properties of the tectorial membrane measured with osmotic stress, *Biophys J* **91**: 2356–2370.

McDonald, J. C., Duffy, D. C., Anderson, J. R., Chiu, D. T., Wu, H., Schueller, O. J. and Whitesides, G. M. (2000). Fabrication of microfluidic systems in (poly)dimethylsiloxane, *Electrophoresis* **21**: 27–40.

McDonald, J. C. and Whitesides, G. W. (2002). Poly(dimethylsiloxane as a material for fabricating microfluidic devices, *Acc Chem Res* **35**: 491–499.

McGuirt, W., Prasad, S., Griffith, A., Kunst, H., Green, G., Shpargel, K., Runge, C., Huybrechts, C., Mueller, R., Lynch, E., King, M.-C., Brunner, H., Cremers, C., Takanosu, M., Li, S.-W., Arita, M., Mayne, R., Prockop, D., Van Camp, G. and Smith, R. (1999). Mutations in COL11A2 cause non-syndromic hearing loss (DFNA13), *Nat Genet* **23**: 413–419.

Mendler, M., Eich-Bender, S. G., Vaughan, L., Winterhalter, K. H. and Bruckner, P. J. (1989). Cartilage contains mixed fibrils of collagen types ii, ix, and xi, *Cell Biol.* **108**: 191–197.

Mountain, D. C. and Cody, A. R. (1999). Multiple modes of inner hair cell stimulation, *Hear Res* **132**: 1–14.

Muller, M., von Hunerbein, K., Hoidis, S. and Smolders, J. W. (2005). A physiological frequency-place map of the cochlea in the cba/j mouse, *Hear Res* **202**: 63–73.

Neely, S. T. and Kim, D. O. (1986). A model for active elements in cochlear biomechanics, *J Acoust Soc Am* **79**: 1472–1480.

Neely, S. T. and Kim, K. O. (1983). An active cochlear model showing sharp tuning and high sensitivity, *Hear Res* **9**: 123–130.

Nowotny, M. and Gummer, A. W. (2006). Nanomechanics of the subtectorial space caused by electromechanics of cochlear outer hair cells, *Proc Natl Acad Sci USA* **103**: 2120–2125.

Patuzzi, R. (1996). Cochlear micromechanics and macromechanics, *in* P. Dallos, A. N. Popper and R. R. Fay (eds), *The Cochlea*, Vol. 8 of *Springer Handbook of Auditory Research*, Springer-Verlag, New York.

Pickles, J. O. and Corey, D. P. (1992). Mechanoelectric transduction by hair cells, *Trends Neurosci* **15**: 254–259.

Quinn, T. M. and Grodzinsky, A. J. (1993). Longitudinal modulus and hydraulic permeability of poly(methacrylic acid) gels: Effects of charge density and solvent content, *Macromolecules* **26**: 4332–4338.

Reuter, G., Gitter, A. H., Thurm, U. and Zenner, H. P. (1992). High frequency radial movements of the reticular lamina induced by outer hair cell motility, *Hear Res* **60**: 236–246.

Rhode, W. S. and Recio, A. (2000). Study of mechanical motions in the basal region of the chinchilla cochlea, *J Acoust Soc Am* **107**: 3317–3332.

Richardson, G. P., Russel, I. J., Duance, V. C. and Bailey, A. J. (1987). Polypeptide composition of the mammalian tectorial membrane, *Hear Res* **25**: 45–60.

Richter, C. P., Emadi, G., Getnick, G., Quesnel, A. and Dallos, P. (2007). Tectorial membrane stiffness gradients, *Biophys J* **93**: 2265–2276.

Robles, L. and Ruggero, M. A. (2001). Mechanics of the mammalian cochlea, *Physiol Rev* **81**: 1305–1352.

Russell, I. J. and Nilsen, K. E. (1997). The location of the cochlear amplifier: spatial representation of a single tone on the guinea pig basilar membrane, *Proc Natl Acad Sci USA* **97**: 2660–2664.

Russell, I., Legan, P. K., Lukashkina, V. A., Lukashkin, A. N., Goodyear, R. J. and Richardson, G. (2007). Sharpened cochlear tuning in a mouse with a genetically modified tectorial membrane, *Nat Neurosci* **10**: 215–223.

Scherer, M. P. and Gummer, A. W. (2005). Vibration pattern of the organ of corti up to 50 khz: evidence for resonant electromechanical force, *Proc Natl Acad Sci USA* **101**: 17652–17657.

Shah, D., Freeman, D. and Weiss, T. (1995). Osmotic response of the isolated, unfixed mouse tectorial membrane to isosmotic solutions: Effect of Na^{+}, K^{+}, and Ca^{+2} concentration, *Hear Res* **87**: 187–207.

Shoelson, B., Dimitriadis, E., Cai, H., Kachar, B. and Chadwick, R. (2004). Evidence and implications of inhomogeneity in tectorial membrane elasticity, *Biophys J* **87**: 2768–2777.

Simmler, M., Cohen-Salmon, M., El-Amraoui, A., Guillaud, L., Benichou, J., Petit, C. and Panthier, J. (2000). Targeted disruption of *otog* results in deafness and severe imbalance, *Nat Genet* **24**: 139–143.

Steel, K. P. (1983a). Donnan equilibrium in the tectorial membrane, *Hear Res* **12**: 265–272.

Steel, K. P. (1983b). The tectorial membrane in mammals, *Hear Res* **9**: 327–359.

Suzuki, H., Lee, Y. C., Tachibana, M., Hozawa, K., Wataya, H. and Takasaka, T. (1992). Quantitative carbohydrate analyses of the tectorial and otoconial membranes of the guinea pig, *Hear Res* **60**: 45–52.

Thalmann, I., Machiki, K., Calabro, A., Hascall, V. and Thalmann, R. (1993). Uronic acid-containing glycosaminoglycans and keratan sulfate are present in the tectorial membrane of the inner ear: Fuctional implications, *Arch Biochem Biophys* **307**: 391–396.

Thalmann, I., Thallinger, G., Comegys, T., Crouch, E. C., Barrett, N. and Thalmann, R. (1987). Composition and supramolecular organization of the tectorial membrane, *Laryngoscope* **97**: 357–367.

von Békésy, G. (1960). *Experiments in Hearing*, McGraw-Hill, New York.

Weiss, T. F. and Freeman, D. M. (1997a). Equilibrium behavior of an isotropic polyelectrolyte gel model of the tectorial membrane: Effect of pH, *Hear Res* **111**: 55–64.

Weiss, T. F. and Freeman, D. M. (1997b). Equilibrium behavior of an isotropic polyelectrolyte gel model of the tectorial membrane: The role of fixed charge, *Aud Neurosci* **3(4)**: 351–361.

Whitesides, G. M., Ostuni, E., Takayama, S., Jiang, X. and Ingber, D. . (2001). Soft lithography in biology and biochemistry, *Annu Rev Bio Eng* **3**: 335–373.

Xue, S., Mountain, D. C. and Hubbard, A. E. (1995). Electrically evoked basilar membrane motion, *J Acoust Soc Am* **97**: 3030–3041.

Zwislocki, J. J. and Cefaratti, L. K. (1989). Tectorial membrane II: Stiffness measurements in vivo, *Hear Res* **42**: 211–228.

Zwislocki, J. J. and Kletsky, E. J. (1979). Tectorial membrane: A possible effect on frequency analysis in the cochlea, *Science* **204**: 639–641.

Zwislocki, J. J. and Kletsky, E. J. (1980). Micromechanics in the theory of cochlear mechanics, *Hear Res* **2**: 505–512.